NASA Tech Briefs

National Aeronautics and
Space Administration

Electronic Components and Circuits

Electronic Systems

Physical Sciences

Materials

Computer Programs

Mechanics

Machinery

Fabrication Technology

Mathematics and Information Sciences

Life Sciences

INTRODUCTION

Tech Briefs are short announcements of innovations originating from research and development activities of the National Aeronautics and Space Administration. They emphasize information considered likely to be transferable across industrial, regional, or disciplinary lines and are issued to encourage commercial application.

Availability of NASA Tech Briefs and TSPs

Requests for individual Tech Briefs or for Technical Support Packages (TSPs) announced herein should be addressed to

National Technology Transfer Center
Telephone No. **(800) 678-6882** or via World Wide Web at **www2.nttc.edu/leads/**

Please reference the control numbers appearing at the end of each Tech Brief. Information on NASA's Commercial Technology Team, its documents, and services is also available at the same facility or on the World Wide Web at **www.nctn.hq.nasa.gov**.

Commercial Technology Offices and Patent Counsels are located at NASA field centers to provide technology-transfer access to industrial users. Inquiries can be made by contacting NASA field centers and program offices listed below.

NASA Field Centers and Program Offices

Ames Research Center
Carolina Blake
(650) 604-0893 or
cblake@mail.arc.nasa.gov

Dryden Flight Research Center
Lee Duke
(805) 258-3802 or
lee.duke@dfrc.nasa.gov

Goddard Space Flight Center
George Alcorn
(301) 286-5810 or
galcorn@gsfc.nasa.gov

Jet Propulsion Laboratory
Merle McKenzie
(818) 354-2577 or
merle.mckenzie@ccmail.jpl.nasa.gov

Johnson Space Center
Hank Davis
(281) 483-0474 or
hdavis@gp101.jsc.nasa.gov

John F. Kennedy Space Center
Gale Allen
(407) 867-6626 or
galeallen-1@ksc.nasa.gov

Langley Research Center
Dr. Joseph S. Heyman
(804) 864-6006 or
j.s.heyman@larc.nasa.gov

Glenn Research Center
Larry Viterna
(216) 433-3484 or
cto@lerc.nasa.gov

George C. Marshall Space Flight Center
Sally Little
(256) 544-4266 or
sally.little@msfc.nasa.gov

John C. Stennis Space Center
Kirk Sharp
(228) 688-1929 or
ksharp@ssc.nasa.gov

NASA Program Offices
At NASA Headquarters there are seven major program offices that develop and oversee technology projects of potential interest to industry:

Carl Ray
Small Business Innovation Research Program (SBIR) & Small Business Technology Transfer Program (STTR)
(202) 358-4652 or
cray@mail.hq.nasa.gov

Dr. Robert Norwood
Office of Aeronautics and Space Transportation Technology (Code R)
(202) 358-2320 or
rnorwood@mail.hq.nasa.gov

John Mulcahy
Office of Space Flight (Code MP)
(202) 358-1401 or
jmulcahy@mail.hq.nasa.gov

Gerald Johnson
Office of Aeronautics (Code R)
(202) 358-4711 or
g_johnson@aeromail.hq.nasa.gov

Bill Smith
Office of Space Science (Code S)
(202) 358-2473 or
wsmith@sm.ms.ossa.hq.nasa.gov

Roger Crouch
Office of Microgravity Science Applications (Code U)
(202) 358-0689 or
rcrouch@hq.nasa.gov

Granville Paules
Office of Mission to Planet Earth (Code Y)
(202) 358-0706 or
gpaules@mtpe.hq.nasa.gov

NASA TechBriefs

National Aeronautics and Space Administration

June 1999
99-06

BLANK PAGE

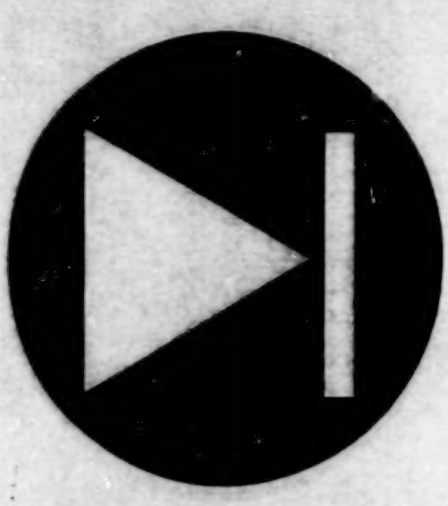

Electronic Components and Circuits

Hardware, Techniques, and Processes

BLANK PAGE

Transmissive Surface-Plasmon Light Valves

Colors in transmissive flat-panel display devices would be voltage-tunable.

NASA's Jet Propulsion Laboratory, Pasadena, California

Transmissive light valves based on voltage-tunable color-selective absorption of light in surface plasmons are undergoing development. Like other surface-plasmon-based devices reported in a number of recent articles in *NASA Tech Briefs*, these light valves could be constructed in many different configurations and concatenated with other optical and electronic components to produce a variety of display and color-filtering devices. These devices would be compatible with, and could be incorporated into, monolithic integrated circuits for use in display, addressing, and interface applications.

As shown in Figure 1, a basic transmissive surface-plasmon light valve would include a substrate made of glass or other suitable transparent material, a metal film (e.g., a thin layer of metal or of indium tin oxide), a layer of electro-optical material (typically a liquid crystal), and another metal film as top electrode. White light would be introduced from the bottom; some of this light would pass through the bottom electrode and impinge on the top electrode, where it would excite surface plasmons at the interface between the metal films and the liquid crystal.

The surface plasmons would absorb some light in a resonance wavelength band determined partly by the index of refraction of the electro-optical material. The light not absorbed in the surface plasmons would pass through the top metal film. The color of this transmitted light would be complementary to that of the reflected light. As in the previously reported surface-plasmon devices, the index of refraction of the electro-optical material, and thus the absorption wavelength band, would depend on the electric field imposed by applying an electric potential between the electrodes. Therefore, one could control the transmitted complementary color by controlling the applied voltage.

Figure 2 illustrates part of a flat-panel display device comprising one of the many different possible combinations of surface-plasmon light valves. This device would be similar to that of Figure 1, except that the lower electrode would be divided into segments that could, for example, correspond to pixels of a display. The colors in each segment could be controlled, independently of the other segments, by applying a distinct voltage between the common upper electrode and the lower electrode for that segment. The electronic circuitry for controlling the voltages on the lower electrode segments could be fabricated on the transparent substrate.

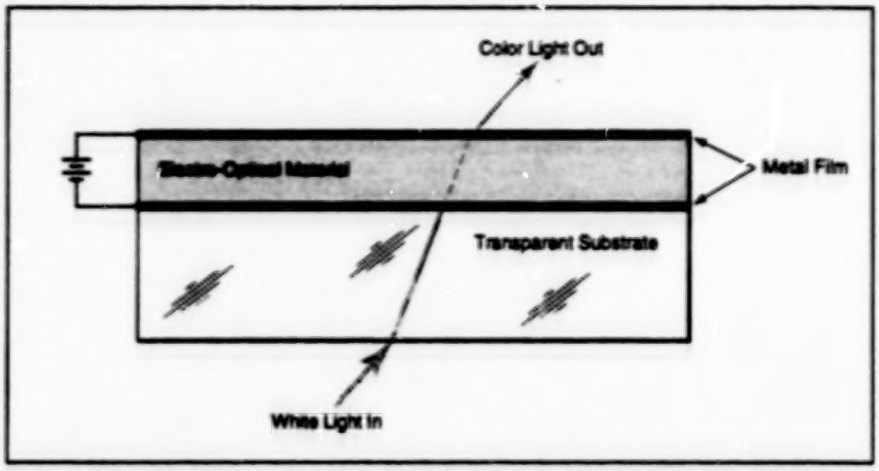

Figure 1. This Light Valve would exploit voltage-tunable color-selective absorption of light in surface plasmons. Light of the color complementary to that of the surface-plasmon absorption resonance would be transmitted.

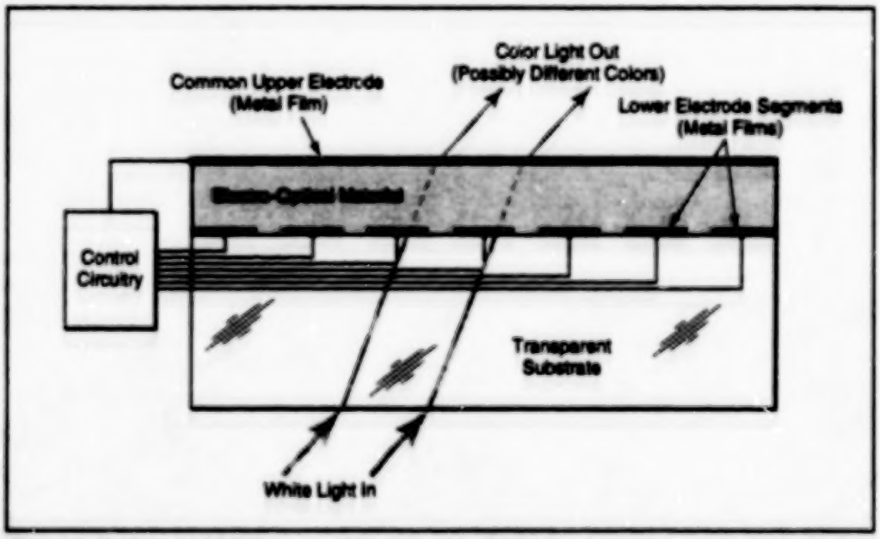

Figure 2. Multiple Light Valves could be arrayed by fabricating a common upper electrode plus multiple side-by-side lower electrode segments. The voltage applied between the common upper electrode and each lower electrode segment would control the color of light transmitted through that segment.

This work was done by Yu Wang, Randy Shimabukuro, and Stephen Russell of Caltech for **NASA's Jet Propulsion Laboratory.** *Further information is contained in a TSP [see page 1].*

In accordance with Public Law 96-517, the contractor has elected to retain title to this invention. Inquiries concerning rights for its commercial use should be addressed to

Technology Reporting Office
JPL
Mail Stop 122-116
4800 Oak Grove Drive
Pasadena, CA 91109
(818) 354-2240

Refer to NPO-20280, volume and number of this NASA Tech Briefs *issue, and the page number.*

Satellite Radio Relay Internet Link for the South Pole

The connection is made via the Tracking and Data Relay Satellite System (TDRSS).

Goddard Space Flight Center, Greenbelt, Maryland

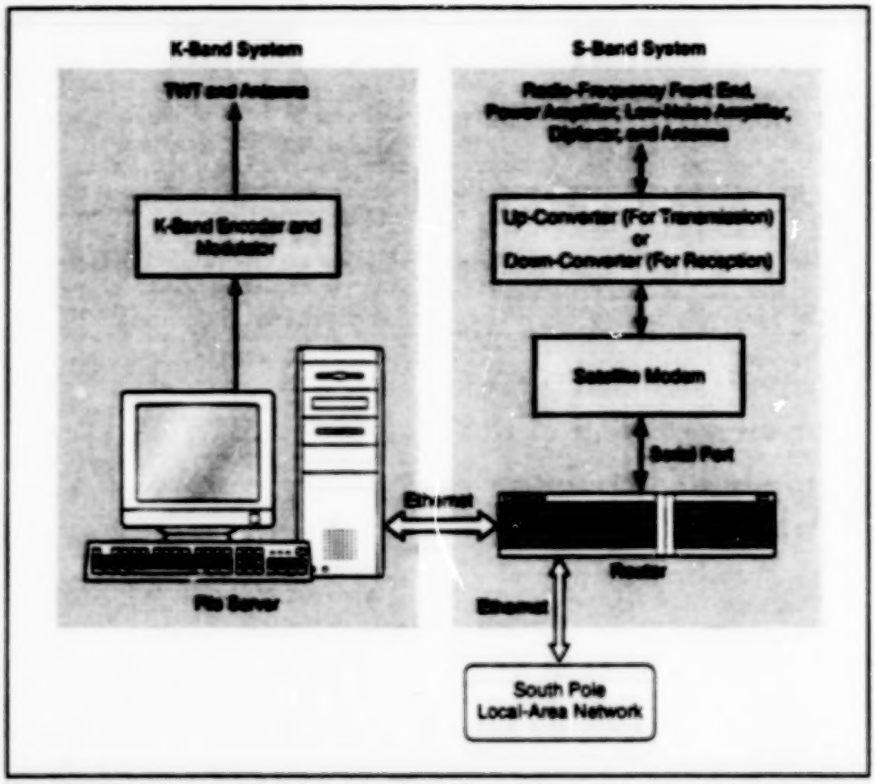

The TDRSS Internet Link Terminal at the South Pole station is a set of equipment that transmits and receives IP traffic, using the TDRSS as a radio relay.

The South Pole TDRSS Relay (SPTR) is a satellite radio relay communication system that provides an Internet link for a station at the South Pole. As the name of the system suggests, the radio connection is made via the TDRSS. The northern end of the link is located at the TDRSS ground-terminal complex at White Sands Test Facility.

The concept of a radio link with the Internet is not new; what is new here is the use of the TDRSS for transmission and reception of data at high speed according to the Internet Protocol (IP).

The visibility of Tracking and Data Relay Satellite 1 (TDRS-1) from the South Pole was a consideration in the choice of the TDRSS (instead of another satellite system) for the SPTR; the inclination (>9.5 °) of the orbit of TDRS-1 makes this satellite visible from the South Pole for more than 3.5 hours each day, and the period of visibility is expected to increase in the long term. In addition, the capabilities of the TDRSs are greater than those of other satellites visible from the South Pole.

The SPTR was designed to provide the following services:

- K-band transmission of data from the South Pole to White Sands at a rate up to 50 Mb/s,
- K-band file-transfer service from the South Pole to White Sands at a rate between 2 and 10 Mb/s, and
- S-band bidirectional IP service at a rate of 1.024 Mb/s.

The SPTR was installed in December 1997. By the next month, it was fully operational, providing the services listed above. Both the South Pole and White Sands terminals were assembled from mostly commercially available equipment. The South Pole equipment (see figure) includes the following:

K-Band Subsystem

- file-server computer
- convolutional encoder
- binary phase-shift keying (BPSK) modulator
- 20-W traveling-wave-tube (TWT) amplifier
- 4-ft (1.2-m) antenna.

S-Band Subsystem

- router
- satellite modem
- up- and down-converters
- 10-W power amplifier
- 4-ft (1.2-m) antenna.

The SPTR additions to the White Sands ground terminal include the following:

- new 1.024-Mb/s connection between the terminal and the Internet
- file-server computer for K-band transfers and the Internet File Transfer Protocol (FTP)
- router for connections among the Internet, the TDRSS, and a local-area network (LAN)
- TDRSS interface that provides coding, scrambling, and descrambling.

The main advantage of the SPTR is that it provides high-level Internet service between the South Pole and other locations. Any IP software can be used, and it is possible to make full use of commercial standards and new developments consistent with the IP. The only major disadvantages are that satellite-communication delays affect the bidirectional IP service and that radio-communication noise could raise the bit-error rate beyond the maximum allowable level of 10^{-5}. The basic SPTR concept could be applied to establish Internet links at field camps and aboard balloons and airplanes.

This work was done by David J. Israel of **Goddard Space Flight Center**. *Further information is contained in a TSP [see page 1].*
GSC-14037

Pixel-Summing APS Imager With Differential Column Readout

Fixed pattern noise and temporal circuit noise are reduced.

NASA's Jet Propulsion Laboratory, Pasadena, California

A complementary metal oxide/semiconductor (CMOS) integrated-circuit video image detector of the active-pixel-sensor (APS) type has been designed to implement programmable multiresolution output (through summing of outputs from selected groups of neighboring pixels) in a low-power, high-speed, low-noise differential column-readout scheme. This scheme

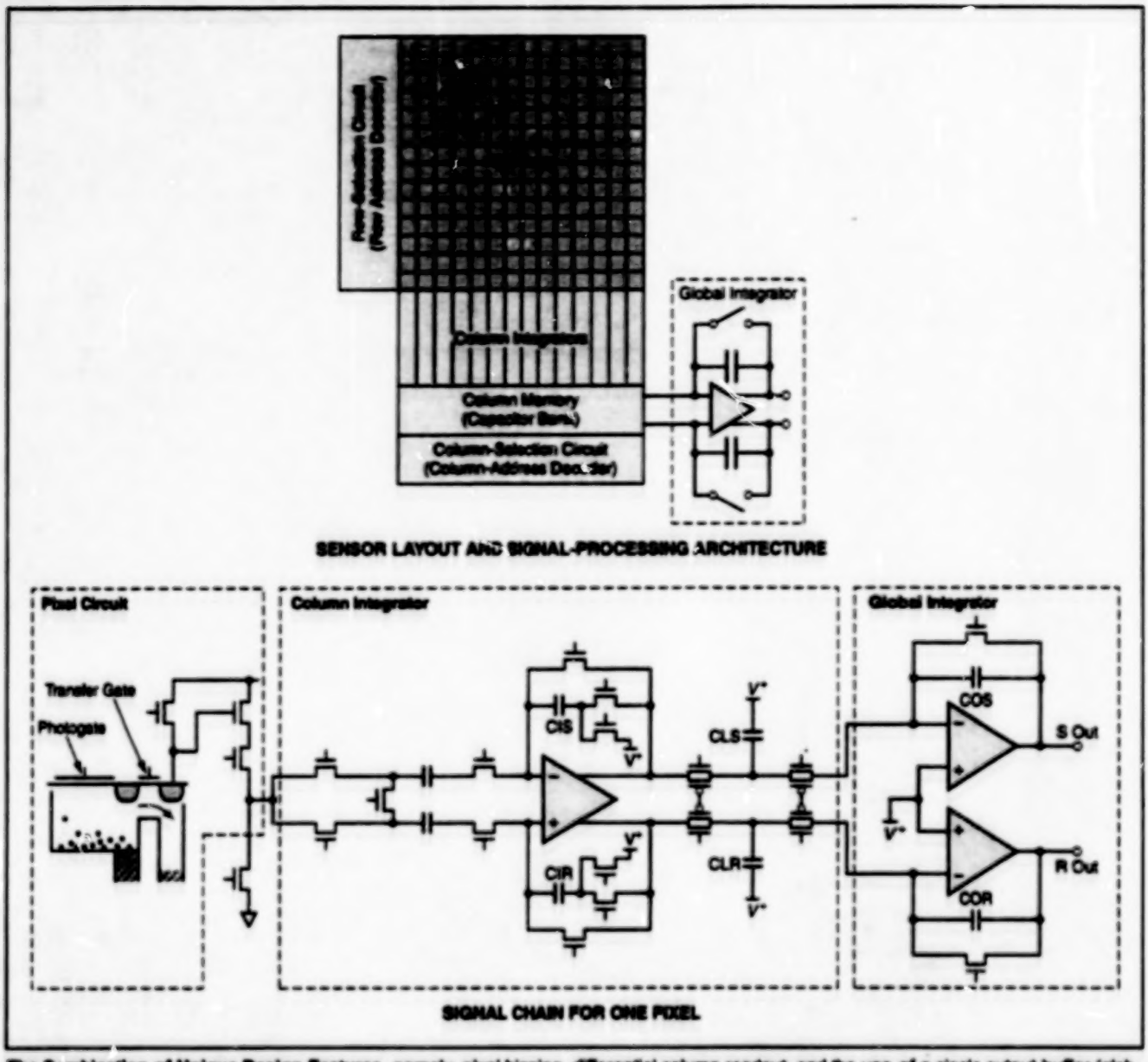

The Combination of Unique Design Features, namely, pixel binning, differential column readout, and the use of a single output buffer (global integrator) reduces output noise.

increases (relative to CMOS APS devices of older designs) the signal-to-noise ratios achievable under low illumination.

Summing of signals from neighboring pixels, also called "pixel binning," amounts to trading away spatial resolution to increase sensitivity or decrease noise. This concept was described in "Active-Pixel Image Sensors With Programmable Resolution" (NPO-19510), *NASA Tech Briefs*, Vol. 20, No. 5 (May 1996), page 26. Pixel binning was implemented previously in a CMOS APS designed for frame-transfer operation. That CMOS APS proved to be susceptible to pickup of extraneous noise and to high residual fixed pattern noise (FPN) due to the use of a single-ended column integrator circuit. Moreover, the pixel binning was implemented by use of a two-dimensional-array analog memory circuit that more than doubled the area of the APS integrated-circuit chip. The differential column-readout scheme of the present CMOS APS reduces both FPN and temporal circuit noise. This scheme also eliminates the need for a two-dimensional memory array, thereby facilitating the development of CMOS APS devices with greater numbers of pixels and higher speed of operation.

Like other typical CMOS APS devices, the present one comprises a two-dimensional array of photogates with active pixel and peripheral readout circuits. The selection of rows and columns for programming the dimensions and sequence of summation kernels is effected by use of externally generated control signals fed to row- and column-address decoders. The figure illustrates both the overall unique signal-processing architecture and the portion of the circuitry in the signal chain from one pixel to the output terminals.

To begin the pixel-summing process for a neighborhood of m by n pixels, each column integrator generates a sum of differential outputs from the pixels in the n selected contiguous rows in that column, in the following procedure: The signal (S) and reset (R) levels of each row are first sampled on the sample-and-hold capacitors CMS and CMR, respectively, as the column integrators are reset. Then the S and R levels are then differentially integrated on integrating capacitors CIS and CIR, respectively. The foregoing steps are repeated until the signals from all m rows

in the neighborhood have been summed. The integrated levels are then sampled and held on the column memory capacitors CLS and CLR. A global integrator generates a differential output signal, one neighborhood at a time, by summing the signals from the memory capacitors of the *n* selected columns. The imager chip dissipates only 24 mW of power while running at 125 frames per second.

This work was done by Bedabrata Pain, Zhimin Zhou, and Eric Fossum of Caltech for **NASA's Jet Propulsion Laboratory**. *Further information is contained in a TSP [see page 1].*

In accordance with Public Law 96-517, the contractor has elected to retain title to this invention. Inquiries concerning rights for its commercial use should be addressed to

Technology Reporting Office
JPL
Mail Stop 122-116
4800 Oak Grove Drive
Pasadena, CA 91109
(818) 354-2240

Refer to NPO-20344, volume and number of this NASA Tech Briefs issue, and the page number.

Cheaper, Lighter Biplates for Methanol Fuel Cells

The main bodies of the plates would be molded from polymers.

NASA's Jet Propulsion Laboratory, Pasadena, California

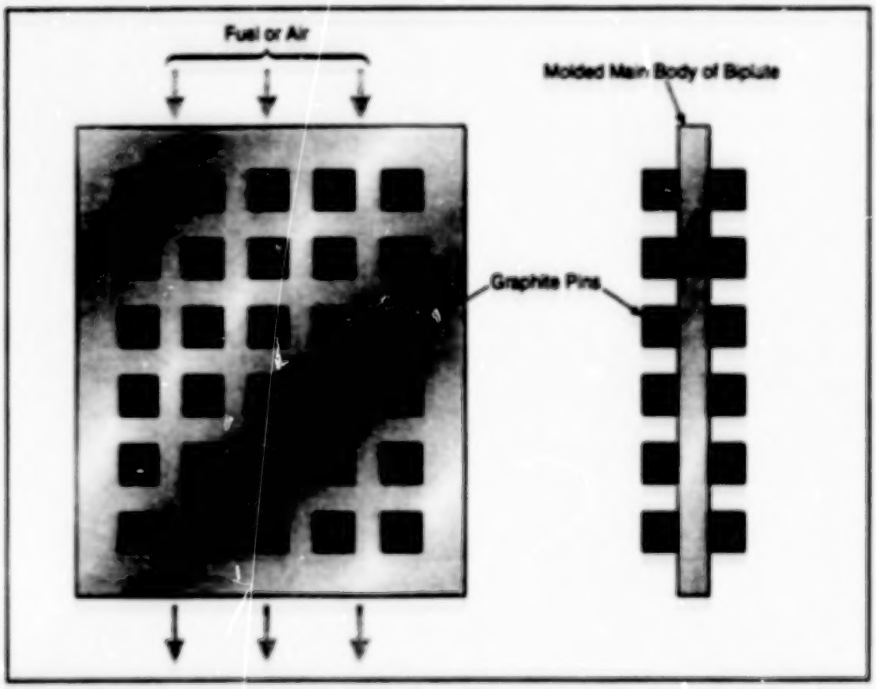

A Biplate Could Be Made of a plastic main body molded around graphite pins, instead of machined from a solid block of graphite. The molded plate with pins would cost and weigh less.

Relatively inexpensive, lightweight biplates for methanol fuel cells have been proposed. The reductions in weight and cost, relative to biplates now used in methanol fuel cells, would be achieved by use of a combination of modified geometry, cheaper and lighter materials, and cheaper manufacturing processes.

A typical methanol fuel cell includes a number of membrane/electrode assemblies (MEAs) stacked in alternation with biplates. Each biplate serves (1) partly as an electrical contact between the cathode of the MEA on one side and the anode of the MEA on the other side, (2) partly as a fuel-and-oxidizer-delivery manifold, (3) partly as an exhaust manifold, and (4) partly as a heat exchanger to remove waste heat. The biplate contains channels for circulating air past the cathode, plus other channels for circulating the fuel solution (methanol dissolved in water) past the anode. The flowing aqueous methanol solution, which is 97 weight percent water, can be used to remove the waste heat.

Heretofore, biplates in methanol fuel cells have been fabricated by machining them out of graphite. About one-third of the cost of a typical methanol cell is incurred in conjunction with the machined graphite biplate(s). In addition, graphite has a density of about 2.0, whereas some other materials that could be used in biplates have lower densities. Thus, if one could reduce the costs of biplates and make them of less-dense materials (plastics), one could effect significant reductions in the costs and weights of methanol fuel cells.

One reason for using graphite until now is that graphite has the required electrical conductivity. A plastic biplate by itself would not be electrically conductive, but the design could be modified to use electrically conductive pins inserted through the thickness of the biplate to provide electrical contact between the anode on one side and the cathode on the other side. The modified design would feature a "flow-cushion" flow-field configuration; the channels on the cathode and anode sides would be defined by the pins, which would disperse the flows of fuel and air over the electrodes (see figure).

The main body of the biplate, with its channels and holes, could be molded. To obtain the required fluid seals around the pins, the main body could be molded around the pins. A suitable material for the main body of the plate might be mineral-filled phenolic, (better known by the trade name "Bakelite"), which has a density of 1.3. While the graphite pins would increase the average density a bit, the average density would still be considerably less than that of a biplate made solely of graphite.

This work was done by Andrew Kindler of Caltech for **NASA's Jet Propulsion Laboratory**. *Further information is contained in a TSP [see page 1].*

In accordance with Public Law 96-517, the contractor has elected to retain title to this invention. Inquiries concerning rights for its commercial use should be addressed to

Technology Reporting Office
JPL
Mail Stop 122-116
4800 Oak Grove Drive
Pasadena, CA 91109
(818) 354-2240

Refer to NPO-20307, volume and number of this NASA Tech Briefs issue, and the page number.

Electronic Systems

Hardware, Techniques, and Processes

BLANK PAGE

A 640 × 486 Long-Wavelength Infrared Camera

Televisionlike imaging in the long-wavelength infrared is now feasible.

NASA's Jet Propulsion Laboratory, Pasadena, California

Figure 1. A QWIP Camera here is held by hand.

A rectangular integrated-circuit focal-plane array of 640 × 486 GaAs/$Al_xGa_{1-x}As$ quantum-well infrared photodetectors (QWIPs) constitutes the image sensor in an experimental long-wavelength infrared camera. This is the first long-wavelength infrared camera containing photodetectors in a focal-plane array that enables imaging in a format similar to that of standard television. The camera, which is sensitive to wavelengths between 8 and 9 μm, can be operated in a staring, snapshot, or video mode.

Until now, state-of-the-art long-wavelength infrared photodetectors have been made from HgCdTe. Difficulties associated with the HgCdTe material system — especially, nonuniformity of devices in arrays — have prevented the fabrication of HgCdTe photodetectors in 640 × 486 arrays with sufficient pixel-to-pixel uniformity to obtain images of acceptable quality in the 8-to-12-μm region of the infrared spectrum. The development of the present camera was guided by the conjecture that by using large-band-gap materials like GaAs and $Al_xGa_{1-x}As$, which can be grown and processed easily, one should be able to fabricate large, relatively uniform arrays of QWIPs to detect light at wavelengths between 6 and 25 μm.

The QWIPs in the present camera are of the bound-to-quasi-bound type, for which the thermionic component of dark current is less than for other types. [This topic was discussed in more detail in "Bound-to-Quasi-Bound Quantum-Well Infrared Photodetectors" (NPO-19633), *NASA Tech Briefs*, Vol. 22, No. 9 (September 1998), page 54.] The basic multiple-quantum-well (MQW) structure of the QWIP array is a stack of 50 identical quantum-well bilayers. Each bilayer comprises (1) a 45-Å-thick well layer of GaAs n-doped at a density $\approx 5 \times 10^{17}$ cm^{-3} and (2) a 500-Å-thick barrier layer of $Al_{0.3}Ga_{0.7}As$. The MQW structure is sandwiched between 0.5-μm-thick top and bottom contact layers of GaAs doped similarly to the well layers.

All of the aforementioned layers were grown on a semi-insulating GaAs substrate by molecular-beam epitaxy. A 300-Å-thick $Al_{0.3}Ga_{0.7}As$ stop-etch layer was grown on top of the top contact layer for use in fabricating a cross-grating structure to couple light into the array. [The cross-grating-coupler concept was described in "Cross-Grating Coupling for Focal-Plane Arrays of QWIPs" (NPO-19657), *NASA Tech Briefs*, Vol. 22, No. 1 (January 1998), page 6a.] A 0.7-μm-thick GaAs cap layer was grown on top of the stop-etch layer. The cross-grating structure was fabricated by photolithography and dry chemical etching.

The array of 640 × 486 photodetectors, with a pitch of 25 μm and a pixel size of 18 × 18 $μm^2$, was then formed by wet chemical etching through the MQW layers into the bottom contact layer. The cross gratings on the tops of the detectors thus formed were covered with Au/Ge and Au for ohmic contact and reflection (reflection at the top surface increases photoresponse, inasmuch as the device is operated in a back-illuminated configuration — that is, with illumination through the substrate). Indium bumps were evaporated onto the (Au/Ge)/Au layers, then the bumps

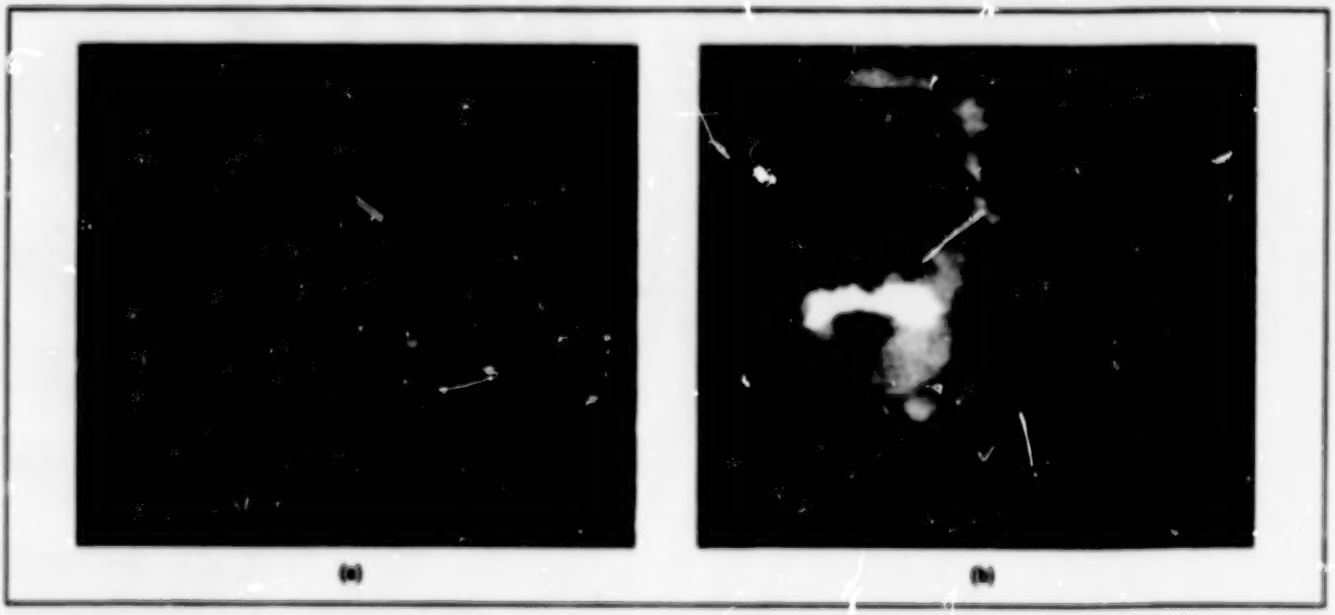

(a) (b)

Figure 2. These Infrared Images were acquired when the camera was cooled to about 70 K and operated at a video frame rate of 30 Hz. The left image taken around midnight shows where the automobiles were parked during the daytime. The right image shows a man's face with a warm mustache, which was heated by a hot-air blower. It also shows hot air emanating from the air blower.

were used to bond (hybridize) the array to a silicon-based complementary metal oxide/semiconductor (CMOS) integrated-circuit 640 × 485 readout multiplexer. The QWIP-array/readout-circuit hybrid was then mounted along with an antireflection-coated, 100-mm-focal-length germanium lens to form the camera (see Figure 1).

In tests, the camera produced excellent images that demonstrated high sensitivity (see Figure 2). The performance of the QWIP operating in a photoconductive (as distinguished from photovoltaic) mode at a reverse bias of 2 V, temperature of 70 K, and background temperature of 300 K was characterized by, among other things, a noise-equivalent differential temperature of 36 mK. The uncorrected nonuniformity (which includes a 1-percent nonuniformity of the readout circuit and a 1.4-percent nonuniformity of a cold stop in front of the array) was found to be only 5.6 percent.

This work was done by Sarath Gunapala, Sumith Bandara, John Liu, and Winn Hong of Caltech for **NASA's Jet Propulsion Laboratory**. *Further information is contained in a TSP [see page 1].*

In accordance with Public Law 96-517, the contractor has elected to retain title to this invention. Inquiries concerning rights for its commercial use should be addressed to

Technology Reporting Office
JPL
Mail Stop 122-116
4800 Oak Grove Drive
Pasadena, CA 91109
(818) 354-2240

Refer to NPO-20312, volume and number of this NASA Tech Briefs *issue, and the page number.*

Improved Computer-Based System for Handling Shuttle Data

Telemetry and command data in 4,800-bit blocks are transmitted in Internet Protocol.

Goddard Space Flight Center, Greenbelt, Maryland

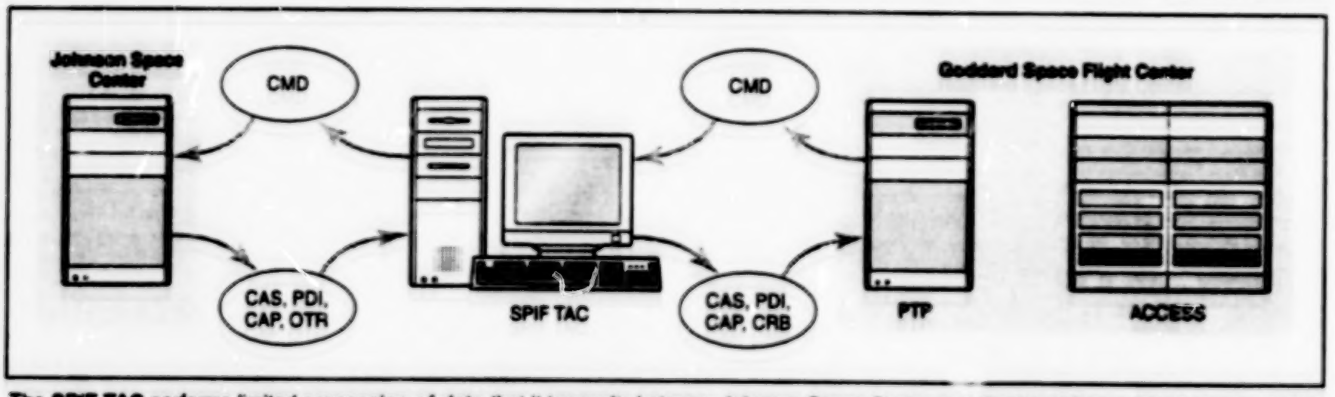

The SPIF TAC performs limited processing of data that it transmits between Johnson Space Center and Goddard Space Flight Center. (CMD is command and PTP is programmable telemetry processor.)

The Shuttle Projects Information Frontier (SPIF) Telemetry and Command Processor (TAC) is a personal-computer-based data-handling system that serves as part of an interface for transfer of data between Johnson Space Center and Goddard Space Flight Center (see figure). The data in question pertain to and/or are acquired by payloads that are carried, launched, deployed, repaired, retrieved, or returned by the Space Shuttle Program.

The SPIF TAC receives and transmits NASA communications (NASCOM) blocks encapsulated in user datagram protocol (UDP) packets. The SPIF TAC receives payload data interleaver (PDI), calibrated ancillary system (CAS), and command acceptance pattern (CAP) data from the mission control center (MCC) at Johnson Space Center and performs limited processing before passing the data to the advanced carrier customer equipment support system (ACCESS) in the Attached Shuttle Payloads Center (ASPC) at Goddard Space Flight Center. In turn, the ACCESS sends commands to the SPIF TAC for validation before transmission to the MCC. Should errors arise in the commands, the command response block (CRB) is returned to the ACCESS.

The SPIF TAC supplants an older system called the "SPIF RS" (RS meaning replacement system). It became necessary to replace the SPIF RS with the SPIF TAC because the SPIF RS will not be able to function after the beginning of the year 2000 and cannot handle the transition to NASCOM Internet Protocol (IP). Because of considerations of cost and schedule, it was decided to design a new system (the SPIF TAC) rather than modify the SPIF RS.

Unix workstations in the SPIF RS were replaced with relatively inexpensive, low-maintenance desktop personal computers in the SPIF TAC. The software for the SPIF TAC was developed by use of Microsoft Visual C++ 5.0. Because of this use of commercial off-the-shelf software, the total cost of development was one-tenth of the cost of replacing the old Unix computers with new Unix computers. In addition, the development was completed in one-fourth of the projected time.

The SPIF TAC is ready for the year 2000 and uses IP to communicate with NASCOM. As an added bonus, the SPIF TAC outperformed the SPIF RS while being tested during the STS-87 space shuttle mission.

This work was done by John A. McQueen, Matthew J. Erb, and Amit K. Singh of AlliedSignal Technical Services Corp. for **Goddard Space Flight Center**. *No further documentation is available.*

GSC-14011

Improved Ultrasonic Imaging of Microscopic Devices

Critical interior bonds could be inspected.

Goddard Space Flight Center, Greenbelt, Maryland

Advances in time gating of ultrasonic signals in scanning acoustic microscopes have been proposed to enable detailed nondestructive examination of bonds and other interfaces deep within the interiors of such micromachined objects as high-density integrated electronic circuits and microelectromechanical systems. The capability to perform such examinations could contribute significantly to ensuring ruggedness and long operational lifetimes for electronic circuits, sensors, and actuators that must withstand harsh environments.

A scanning acoustic microscope is usually operated in a C-scan mode, using a pulse-gated acoustic signal with carrier frequency between 50 and 100 MHz. The scan can reveal features at depths up to several millimeters. However, the bonds, interfaces, and other features that are of interest in an assessment of the structural integrity of a micromachined object typically have dimensions of the order of microns, and acoustic signals (pulse echoes) that could be used to analyze these features often appear with similar signals from other features superimposed on them. As a result, it is difficult to assess structural integrity of a feature of interest.

In C-scan acoustic microscopy as it has been practiced until now, the pulse echo from an area of interest is gate-peak-detected to produce the ultrasonic image of that area. When the detection gate interval is set to encompass the entire pulse envelope, the depth resolution of the image is compromised because of the superposition of pulse echoes mentioned above.

The proposed advances in time gating would increase the isolation of the echo signal of interest from the other superimposed signals. One of the proposed advances would exploit the observation that by limiting the duration of the detection gate to a single cycle of the carrier signal, the sharpness of the acoustic image can be increased greatly. If the gate interval contains the echo from a feature of interest, the structural integrity of the feature can be analyzed.

Other advances could include improved sensors and shaping of pulses to increase signal-to-noise ratios. Yet another advance would be the use of a phase-lock loop to track the peak of the pulse echo corresponding to a feature of interest; this would greatly increase the capability for examining complex structures.

This work was done by E. James Chern of **Goddard Space Flight Center**. *Further information is contained in a TSP [see page 1].*

GSC-14092

BLANK PAGE

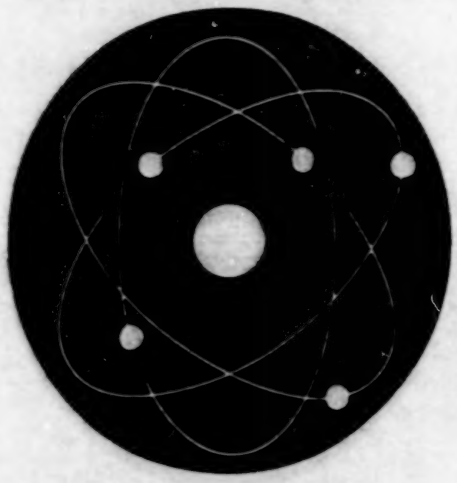

Physical Sciences

Hardware, Techniques, and Processes

BLANK PAGE

Spectral Reflectometer for Quantifying Stress in Plants

Spectral measurements of chlorophyll loss indicate stress levels.

Stennis Space Center, Mississippi

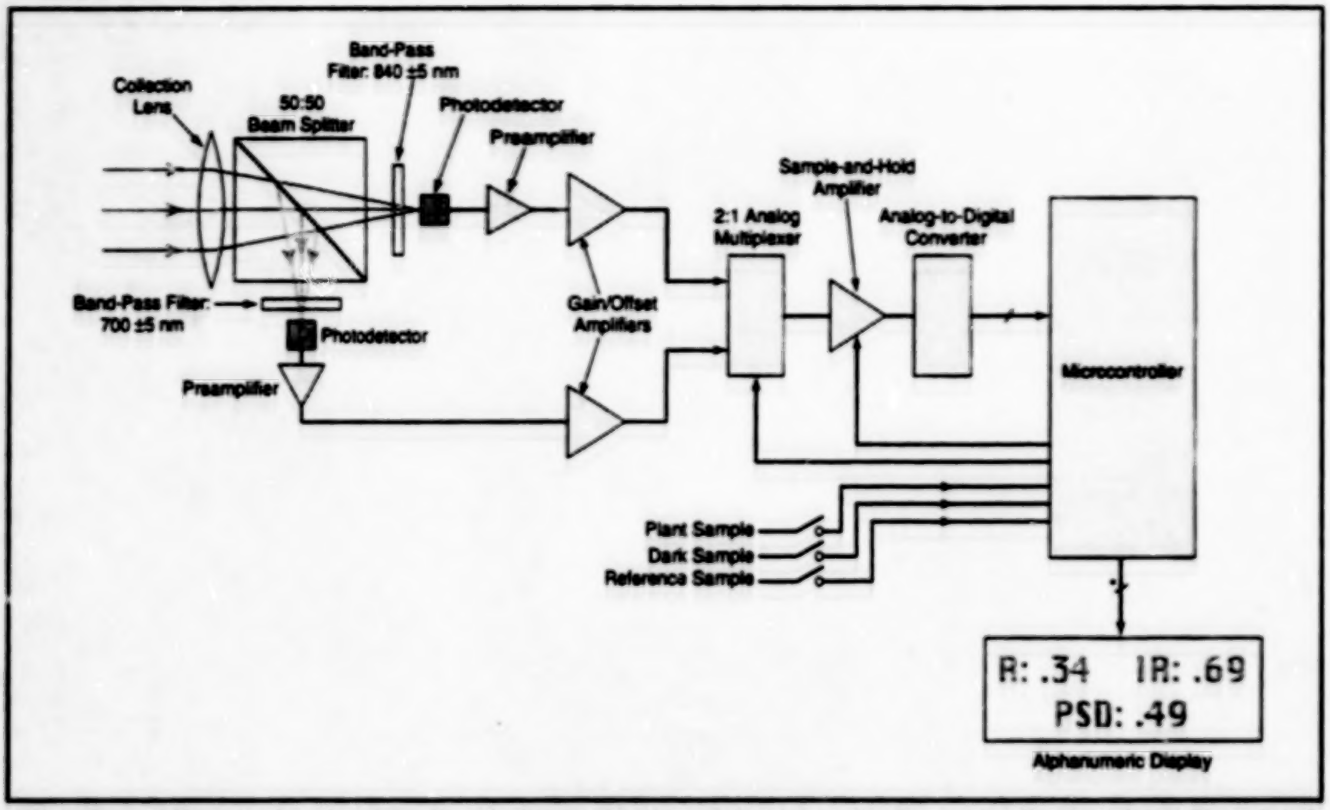

This Instrument Measures the ratio between the reflectances of a plant sample at two wavelengths; one red, the other infrared. The ratio indicates the level of stress in the plant sample.

A hand-held optoelectronic instrument has been designed to generate a quantitative indication of the loss of chlorophyll, and thus the level of stress, in plants. The instrument exploits the known spectral-reflectance characteristics associated with the chlorophyll contents of healthy and unhealthy plants. In particular, the instrument indicates the ratio between the reflectances of plants in narrow spectral bands centered at wavelengths of 700 and 840 nm, respectively. This ratio ranges from about 0.1 for a healthy plant to ≥0.4 for an unhealthy plant. [Other similar instruments have been based on fluorescence (as distinguished from reflectance) ratios, but the intensity of reflected light is much greater than fluorescence intensity at the wavelengths used in this instrument.]

The instrument is operated in the following procedure: Readings are first taken with the instrument aimed at a standard reflectance target. Next, readings are taken with the instrument aimed at the plants of interest. Both the plants and the target could be illuminated by sunlight or artificial light. From time to time, readings are also taken in the dark to obtain corrections for nonzero components of photodetector outputs ("dark currents") at zero illumination.

In the instrument (see figure), light reflected from the plants or target is intercepted by a lens, then split into two beams. One beam is band-pass filtered at a wavelength of 700 nm, the other at a wavelength of 840 nm. Each beam then impinges on a photodetector, which is located with the center of its input face at a focal point of the lens.

The outputs of the photodetectors are amplified and offset as needed. A 2:1 multiplexer selects whichever of the two amplified, offset photodetector outputs is to be fed to a sample-and-hold (S/H) amplifier followed by an analog-to-digital converter (ADC). A microcontroller controls the multiplexer, the S/H amplifier, and the ADC. The digital sample put out by the ADC is fed to the microcontroller for further digital processing in coordination with the acquisition of samples, as described next.

With the instrument aimed at the reflectance target, the operator presses a pushbutton switch marked "reference," causing the microprocessor to command the acquisition of a digital sample, first at the wavelength of 700 nm, then at the wavelength of 840 nm. Five samples are taken and averaged automatically on each channel with the single push of a button, then the sample from the dark reading at that wavelength is subtracted to obtain a corrected reading, which is stored. The instrument is then aimed at the plants of interest, and the operator presses a push-button switch marked "plant sample," causing the microprocessor to command the acquisition and processing of readings from the plants in the same manner as from the reflectance target.

At any time before or after acquiring the reflectance-target or plant readings, the operator could place an opaque cover over the lens and press a pushbutton switch marked "dark sample" to acquire the dark readings. In the same manner as for the reflectance-target and plant readings, five dark readings would be acquired at each wavelength and averaged. The average values would then be stored and used to correct the reflectance-target and plant readings as described above.

The microprocessor divides the corrected plant reading for the wavelength of 700

nm by the corrected reflectance-target reading for that wavelength to obtain the reflectance of the plants at that wavelength [r(700)]. The microprocessor also divides the corrected plant reading for the wavelength of 840 nm by the corrected reflectance-target reading for that wavelength to obtain the reflectance of the plants at that wavelength [r(840)]. Finally, the microprocessor calculates [r(700)/r(840)], which is the desired ratio indicative of stress in the plants.

This work was done by Bruce A. Spiering and Gregory A. Carter of **Stennis Space Center**. *Further information is contained in a TSP [see page 1].*

This invention is owned by NASA, and a patent application has been filed. Inquiries concerning nonexclusive or exclusive license for its commercial development should be addressed to the Patent Counsel, Stennis Space Center [see page 1]. Refer to SSC-00050.

Portable Multispectral Telescope

Optics can be reconfigured relatively easily, and off-the-shelf components can be used.

Stennis Space Center, Mississippi

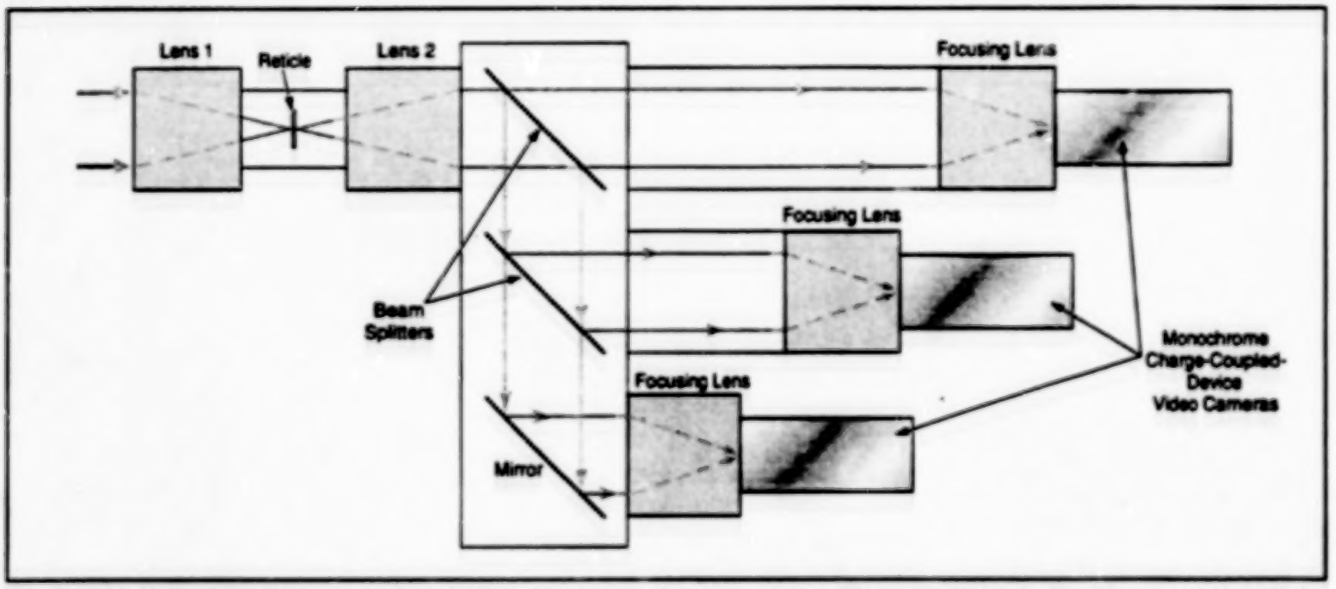

The Portable Multispectral Telescope produces multiple video images of the same scene in different spectral bands. The telescope could readily be configured for more, fewer, or different spectral bands.

A telescope produces multiple video outputs representing coregistered images in multiple spectral bands that can range from ultraviolet through far infrared. Although the overall function of the telescope is partly equivalent to that of a color television camera equipped with telescopic lenses, its basic optical configuration differs from that of a color television camera, and it is designed for different applications. In the original intended application, the telescope will be used in research on remote optical detection of stress in plants. By suitable choice and placement of optical components, as described below, the telescope can readily be configured for other special applications.

Light from the scene under observation enters the telescope along an input telescopic optical path that is common to the multiple output paths (see figure). The input telescopic optical path includes lenses 1 and 2. (As used here, "lenses" is shorthand for optical subsystems that could, optionally, comprise single- or multiple-element lenses or multiple-lens subsystems.) Lens 1 focuses the light to a real image on a reticle, which serves as a common alignment reference for the multiple spectral images. Lens 2 then expands and collimates the light. The collimated beam then enters an assembly of beam splitters, filters, and a mirror. The portion of the collimated beam emerging through each filter in this assembly contains only light in one of the desired spectral bands. A lens on the optical path for each spectral band focuses the collimated light onto the array of photodetectors in a video camera that is dedicated to producing the video image for that band.

Although the configuration shown in the figure is for three spectral bands, other configurations with fewer or more spectral bands could be chosen. The input beam could be split and filtered as many times as needed, subject only to the practical limitation imposed by finitude of the available luminous flux. Lenses, beam splitters, filters, and video cameras can be off-the-shelf or custom-designed, as needed, for imaging in specified spectral bands.

This work was done by Bruce A. Spiering of **Stennis Space Center**. *Further information is contained in a TSP [see page 1].*

This invention is owned by NASA, and a patent application has been filed. Inquiries concerning nonexclusive or exclusive license for its commercial development should be addressed to the Patent Counsel, Stennis Space Center [see page 1]. Refer to SSC-00048.

Portable Video Imager for Detecting Stress in Plants

Multispectral images are processed into images indicative of chlorophyll loss.

Stennis Space Center, Mississippi

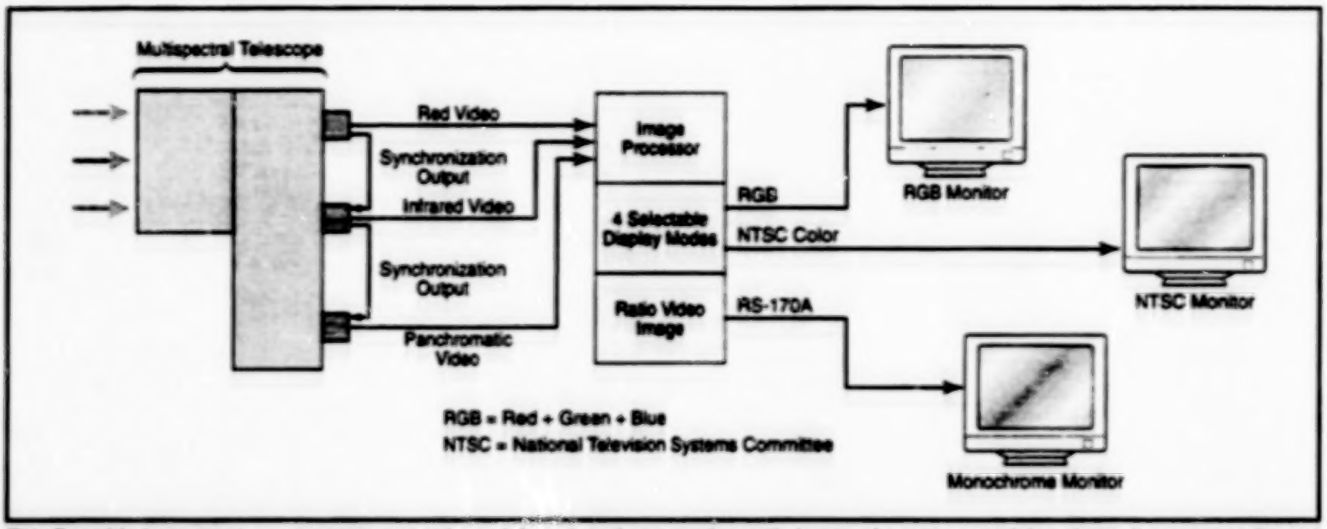

This Portable Instrument can generate one red, one infrared, and one panchromatic image of a scene containing plants. It processes the red and infrared images to obtain ratios between red and infrared reflectances. These ratios are used to control brightness levels in a synthetic video image to indicate levels of stress in the plants.

A portable instrument can generate video images indicative of physiological stress in plants. The instrument exploits the known relationships among physiological stress in plants, loss of chlorophyll, and changes in spectral reflectance. The instrument acquires multispectral video images of a scene that contains plants, digitizes the images, and processes the image data to generate a new image that maps chlorophyll loss in the scene.

The instrument (see figure) is based partly on the instruments described in the two preceding articles, "Spectral Reflectometer for Quantifying Stress in Plants" (SSC-00050) and "Portable Multispectral Telescope" (SSC-00048). It includes a multispectral telescope similar to the one described in the second-mentioned preceding article, with three spectral channels. Two of the channels would contain narrow-band optical filters centered at wavelengths of 700 and 840 nm, respectively. The third channel is left unfiltered to obtain a panchromatic video image. The images in all three channels are collected by identical video cameras, the outputs of which are processed. As explained in the noted prior article about the multispectral telescope, the three video images are inherently coregistered; this is an important advantage in that it eliminates the need for additional registration steps in processing of image data.

A set of image data is acquired with the telescope aimed at the plants of interest, while two reference detectors, one with identical 700-nm filters and one with identical 840-nm filters, are exposed to incident solar radiance. The ratio of the 700-nm image with the 700-nm reference and the ratio of the 840-nm image with the 840-nm reference are being computed as the images are scanned. Then the outputs are ratioed 700–840 nm to create the final output. This ratio is the desired quantity indicative of the amount of chlorophyll lost by the plant part(s) imaged in the pixel. This ratio is used to control local brightness levels in a synthetic image to indicate local contents of chlorophyll. The synthetic chlorophyll image could, if desired, be overlaid on the panchromatic image.

This work was done by Bruce A. Spiering and Gregory A. Carter of **Stennis Space Center.** *Further information is contained in a TSP [see page 1].*

This invention is owned by NASA, and a patent application has been filed. Inquiries concerning nonexclusive or exclusive license for its commercial development should be addressed to the Patent Counsel, Stennis Space Center [see page 1]. Refer to SSC-00049.

Improved HSPES-Based MEAs for Methanol Fuel Cells

Cathode structures and the process used to make them have been modified.

NASA's Jet Propulsion Laboratory, Pasadena, California

Improved membrane/electrode assemblies (MEAs) made partly from hydrogen form of sulfonated polyether sulfone (HSPES) have been developed for use in methanol fuel cells. In comparison with traditional fuel-cell MEAs made partly from a commercial perfluorosulfonic acid-based polymer, these MEAs perform similarly, but cost much less.

Prior to the development reported here, MEAs made partly from HSPES did not perform as well as did the traditional ones. Analysis of polarization data for an HSPES-based MEA revealed that losses in the cathode accounted for the loss in performance. Further analysis guided by previous experience led to the conclusion that the loss in performance was caused by poor utilization of the cathode catalyst. This conclusion, in turn, led to the conjecture that performance might be improved by use of a modified fabrication process that would yield a modified cathode structure, wherein the cathode cata-

lyst would be bonded in an improved way and distributed in different structures, such that a greater proportion of the catalyst loading would participate in electrochemical reactions.

It was conjectured, further, that the best way to improve bonding and reduce migration was to immobilize some of the catalyst prior to a hot-pressing step that is part of the MEA-fabrication process. In a previous version of the process, a paint containing polytetrafluoroethylene, water, and triton was applied to carbon paper and sintered at a temperature of 350 °C under a nitrogen blanket; this immobilized the catalyst. A solution of the perfluorosulfonic acid-based polymer was then applied to the catalyst-covered electrode before hot pressing. One of the goals pursued in the development of this previous version was of the process to obtain adequate performance with a catalyst loading reduced from the value (4 mg/cm^2) of the traditional MEAs. The catalyst loading achieved was 1 mg/cm^2, but, as stated above, performance was below that of traditional MEAs.

In the modified process, the catalyst loading is not reduced from that of traditional MEAs. However, the catalyst is applied in two layers, each containing half (2 mg/cm^2) of the total catalyst loading. The first half of the catalyst is applied as in the previous version of the process and sintered at 350 °C, but unlike in the previous version of the process, the perfluorosulfonic acid-based polymer is not applied after sintering. The second half of the catalyst loading is applied as part of a paint that also contains water and the perfluorosulfonic acid-based polymer. Unlike the first layer, the second layer is not sintered. Instead, the MEA is hot-pressed after application of the second layer.

The two-layer cathode catalytic structure offers advantages over the previous single-sintered-layer cathode catalytic structure:

- The high sintering temperature can reduce the activity of the catalyst. As a result of the placement of the unsintered layer over the sintered one, highly active catalyst is in direct contact with the membrane after hot pressing.
- Quasi-sintering of polytetrafluoroethylene can reduce catalyst activity by covering otherwise active catalytic sites. However, the unsintered layer contains no polytetrafluoroethylene. Because the unsintered layer becomes bonded to the membrane, the lower catalytic activity of the sintered layer becomes less important. For this reason, it might be possible to increase the polytetrafluoroethylene content of the sintered layer to improve the barrier to migration.

The performances of an HSPES-based MEA made by the modified process (improved MEA) and of one made by the previous version of the process were measured in a comparative test. At a current density of 300 mA/cm^2, the MEA made by the previous version of the process exhibited a potential of 212 mV, whereas the improved MEA exhibited a potential of 387 mV.

This work was done by Andrew Kindler and Shiao-Ping Yen of Caltech for **NASA's Jet Propulsion Laboratory**. *Further information is contained in a TSP [see page 1].*

In accordance with Public Law 96-517, the contractor has elected to retain title to this invention. Inquiries concerning rights for its commercial use should be addressed to

Technology Reporting Office
JPL
Mail Stop 122-116
4800 Oak Grove Drive
Pasadena, CA 91109
(818) 354-2240

Refer to NPO-20306, volume and number of this NASA Tech Briefs *issue, and the page number.*

Kit for Sampling Nitrosamines From Aqueous Solutions

Carcinogens to be analyzed can be extracted from groundwater or soil relatively quickly and cheaply.

Lyndon B. Johnson Space Center, Houston, Texas

Scientists at White Sands Test Facility (WSTF) have devised a kit for extracting nitrosamines from aqueous solutions. In comparison with extractions according to the method recommended by the Environmental Protection Agency (EPA), extractions by use of the kit are faster, cheaper and less labor-intensive, and they yield greater recoveries as well as test results that are more accurate. No other nitrosamine test kit performs at the level of this kit while satisfying requirements unique to WSTF.

The nitrosamines found at WSTF are organic compounds. They are powerful carcinogens that are by-products of dimethyl hydrazine, a rocket fuel used at WSTF before the fuel was linked to human cancers. Because the EPA requires suspected groundwater and soil be tested for carcinogens by use of gas chromatography (GC) and because the EPA's method of extraction and preparation of samples for analysis by GC is a labor-intensive method that involves the use of dichloromethane, WSTF scientists developed their own extraction method, which involves the use of the present kit for sampling nitrosamines from aqueous solutions.

In developing the kit, the WSTF scientists improved on sampling kits that were already extant to provide for extraction and concentration of nitrosamines from groundwater or soil analysis into a nitrogen/phosphorous detector prior to GC. Their technique involves passing a sample with a volume of 250-mL through a solid-phase extraction tube that contains 0.5 g of activated charcoal. Experiments have shown that two nitrosamines found at WSTF — N-nitrosodimethylamine (NDMA) and N-nitrosodi-n-propylamine (NDPrA) — collected by this technique and stored in the dark at a temperature of 4 °C are stable for up to 28 days — sufficient time to ship samples for analysis. Once a sample has arrived in a laboratory, NDMA and NDPrA are eluted with 2 mL of acetone and analyzed under conditions detailed in EPA Method 607 and SW-846 Method 8070.

Nitrosamines in groundwater and/or soil can exert adverse effects on human health in production facilities where they are found, and contribute to overall pollution. Because some nitrosamines are powerful human carcinogens, their presence in any place where humans live or work must be of continuing concern to public and private industries. The WSTF sampling kit is expected to be most useful at WSTF, where its sensitivity and accuracy have significantly improved the ability of scientists to detect NDMA and NDPrA, which are two of the three on-site nitrosamines linked to dimethyl hydrazine. The kit could also be used in measuring the effects of production and/or pollution-abatement activities elsewhere, in connection with industrial activities that involve handling of the analytes of rocket fuels.

This work was done by Gary Moffett and Benjamin Greene of Allied Signal for **Johnson Space Center**. *Further information is contained in a TSP [see page 1].*
MSC-22794

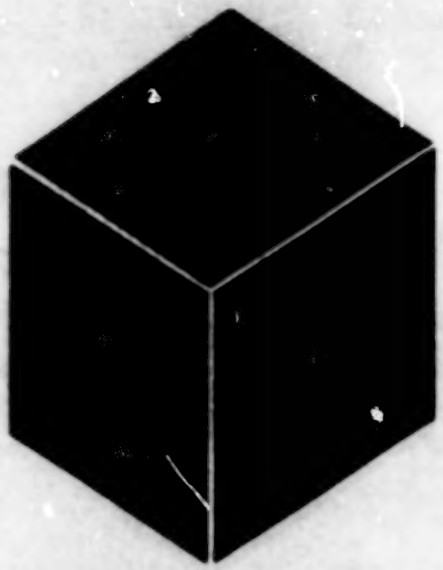

Materials

Hardware, Techniques, and Processes

BLANK PAGE

PSSA/PVDF Polymer Electrolyte Membranes for CH_3OH Fuel Cells

Methanol crossover is reduced, with consequent increases in fuel efficiency and electrical performance.

NASA's Jet Propulsion Laboratory, Pasadena, California

Improved polymer electrolyte membranes for direct methanol fuel cells can be made by any of a variety of processes in which cross-linked polystyrene sulfonic acid (PSSA) is mobilized within electrochemically inert matrices of poly(vinylidene fluoride) (PVDF). Alternatively, other matrix materials can be substituted for, or blended or copolymerized with, PVDF. The principal advantage of these membranes over polymer electrolyte membranes made of other materials is that they are less permeable to methanol; this translates to less crossover of methanol in molecular form (denoted "methanol crossover" for short). Methanol crossover is undesired because it wastes fuel and degrades fuel-cell performance, as explained below.

Figure 1 schematically illustrates a typical direct liquid-feed methanol fuel cell in operation. The polymer electrolyte membrane is part of a membrane/electrode composite-material laminate known in the industry as a membrane/electrode assembly. The anode is preferably made from a carbon-supported Pt/Ru catalyst; the cathode is preferably made from a carbon-supported Pt catalyst. An aqueous solution of methanol is circulated past the anode, while air or oxygen is circulated past the cathode.

Oxidation of methanol at the anode generates carbon dioxide, electrons, and protons. The electrons travel through an external electrical load, to which they deliver the electrical energy generated by the chemical reactions in the fuel cell. The polymer electrolyte membrane serves as a medium for transport of the protons to the cathode, where the protons combine with electrons and oxygen, producing water. To the degree to which the polymer electrolyte membrane allows conduction of electrons, electrical energy is diverted from the external load; and to the degree to which the membrane allows methanol crossover, the methanol fuel is consumed unproductively at the cathode.

It would not be possible, within the limits of this article, to present a comprehensive description of the many alternative materials, techniques, and processes that could be used in fabricating PSSA/PVDF membranes and membrane/electrode assemblies that contain them. The best that can be done here is to present an example of a preferred approach in which (1) a PVDF membrane matrix is prepared; (2) the membrane matrix is impregnated with a solution of styrene, divinylbenzene, and a small amount of a polymerization initiator; (3) the styrene and divinylbenzene are copolymerized within the membrane matrix; (4) the membrane is sulfonated; and (5) the membrane is sandwiched between electrode films.

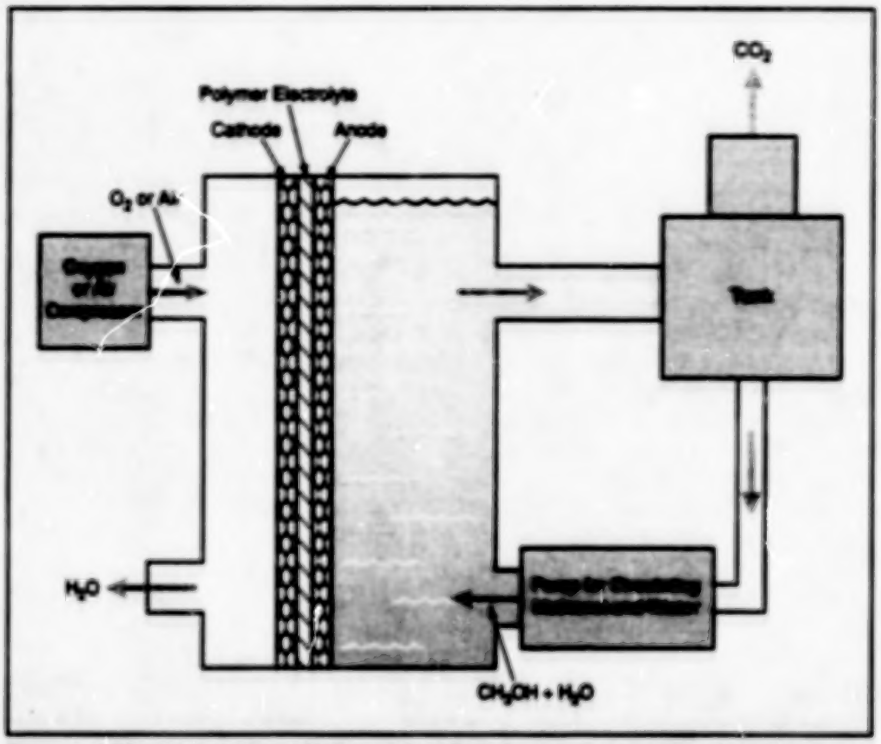

Figure 1. A Direct Liquid-Feed Methanol Fuel Cell depends on a polymer electrolyte membrane for proper operation.

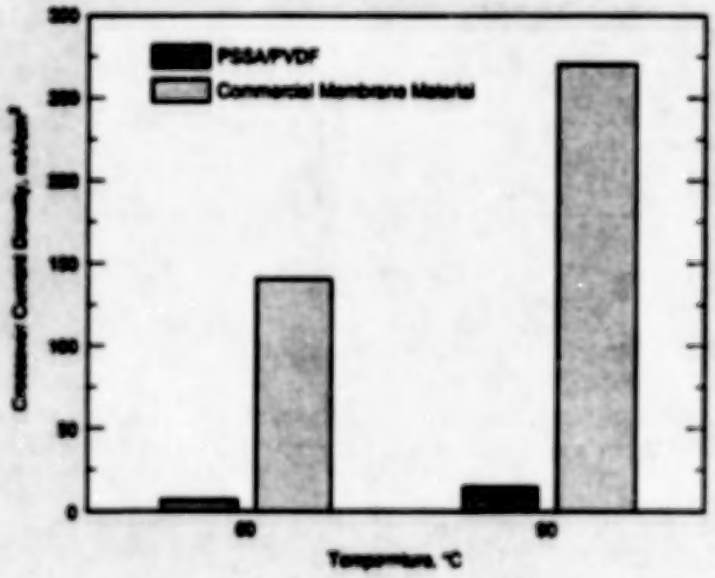

Figure 2. Methanol-Crossover Current Densities were measured in two fuel cells operating with 1.0 M methanol solution circulated past the anodes and oxygen at a pressure of 20 psig (gauge pressure of 138 kPa) circulated past the cathode.

The PVDF membrane matrix can be prepared by hot pressing of PVDF powder or of a PVDF membrane cast from solution. Alternatively, one can start with a commercial film made of PVDF or a copolymer of PVDF and hexafluoropropylene. The membrane matrix is impregnated by immersion in a bath of styrene, divinylbenzene, and azobis(isobutyronitrile) (AIBN) or another suitable polymerization initiator. The proportion of AIBN is typically between 0.3 and 0.4 weight percent. The proportions of styrene and divinylbenzene govern the amount of cross-linking.

After removal from the bath, the membrane is heated to a temperature between 150 and 170 °C and pressed at 500 to 2,000 psi (3.4 to 14 kPa) for as long as it takes to increase the density of the membrane by 15 to 25 percent. The membrane is then sulfonated by immersion in a solution comprising 15 percent of chlorosulfonic acid in chloroform for 24 hours. The sulfonated membrane is washed in distilled water, then hydrolyzed in distilled water at a temperature of 65 °C. At the end of this process, there is a sulfonic acid group attached to almost every aromatic ring in the membrane. A membrane/electrode assembly is then fabricated by hot-pressing the membrane, while it is still in its hydrated state, between catalyzed, polytetrafluoroethylene-impregnated porous carbon electrode layers.

Figure 2 presents an example of experimental data that show that the methanol-crossover rate of a membrane/electrode assembly made with PSSA/PVDF was less than that of one made with an expensive commercial perfluorocarbon proton-exchange membrane that has been the membrane of choice for methanol fuel cells in recent years. Another advantage of a PSSA/PVDF membrane over the commercial membrane arises in connection with oxygen-flow rates. The necessary circulation of oxygen past the cathode undesirably tends to dry the membrane, thereby increasing its electrical resistivity. Therefore, to minimize the drying effect, it is preferable to operate a fuel cell at the smallest feasible oxygen flow. A fuel cell containing a PSSA/PVDF can function well at a small oxygen flow, whereas one containing a membrane of the commercial material performs poorly at a small oxygen flow.

This work was done by G. K. Surya Prakash, George A. Olah, Marshall C. Smart, and Qungie J. Wang of the University of Southern California and Sekharipuram Narayanan of Caltech for **NASA's Jet Propulsion Laboratory**. *Further information is contained in a TSP [see page 1].*

In accordance with Public Law 96-517, the contractor has elected to retain title to this invention. Inquiries concerning rights for its commercial use should be addressed to

Technology Reporting Office
JPL
Mail Stop 122-116
4800 Oak Grove Drive
Pasadena, CA 91109
(818) 354-2240

Refer to NPO-20378, volume and number of this NASA Tech Briefs *issue, and the page number.*

Improved Aerogel-Based Thermal Insulation Systems

Thermal conductivities are generally lower than those achieved previously.

John F. Kennedy Space Center, Florida

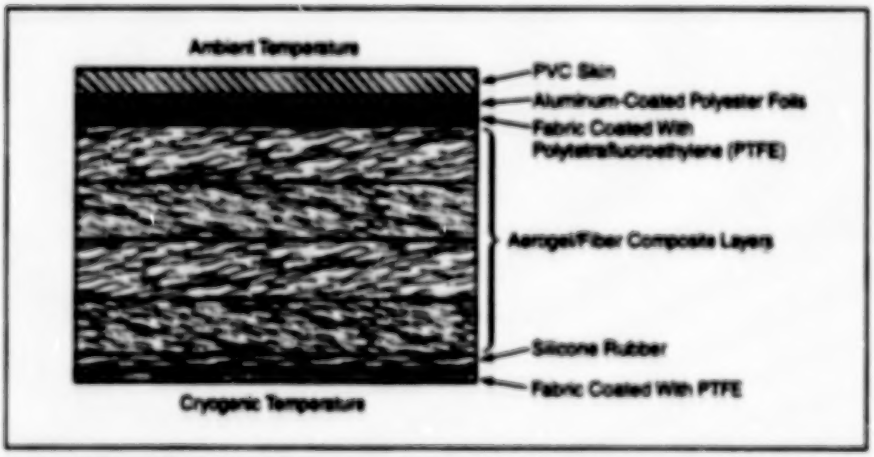

Aerogel-Based Superinsulation contains layers of highly engineered materials, each performing a function that contributes to the overall reduction of heat transfer, to safety, and/or to protection against the environment.

Improved aerogel-based thermal insulation systems have been developed to provide cost-effective and easier-to-handle alternatives to various types of multilayer insulation (MLI) and evacuated powder insulation now used on cryogenic equipment. The apparent thermal conductivities of the aerogel-based systems are comparable to MLI systems and are well below the thermal conductivities of the other systems.

MLI systems are expensive, structurally complex, and bulky; the insulating properties are anisotropic; and maintaining a high vacuum [10^{-4} to 10^{-5} torr (about 10^{-2} to 10^{-3} Pa)] is required in MLI for full insulating effectiveness. Evacuated powder insulation is about one order of magnitude less effective than is MLI, but its insulating properties are isotropic, it is generally easier to install, and it requires only a moderate vacuum [10^{-2} to 10^{-3} torr (about 1 to 10^{-1} Pa)] to realize its full insulation potential. Unfortunately, the powder in evacuated powder insulation tends to settle in response to vibration and thermal cycling, forming voids that act as heat leaks.

The improved aerogel-based insulation systems are composites which can be manufactured in blanket, sleeve, or clamshell forms to be used with or without evacuation. These composite systems take advantage of the low thermal conductivity of the ultra-low-density aerogels to minimize heat transfer and incorporate a flexible, durable matrix to maximize applicability. The core of the system is aerogels formed at the fiber-fiber contacts of the matrix, forcing solid heat-transfer to occur through the aerogels. This composite configuration improves both the ease of handling aerogels and the overall thermal resistance. The closed-packed structure of the aerogels eliminates the open spaces in the fiber matrix and thereby minimizes convection heat transfer. Excellent thermal resistance has been achieved for both evacuated and nonevacuated insulation systems while maintaining good flexibility. The aerogel can also be produced in an opacified fiber matrix to inhibit radiation heat transfer in the infrared range.

A typical insulating system for use on cryogenic equipment is an integrated, layered structure that includes a backing layer on the cold side and protective layers on the warm side (see figure). One of the protective layers is a tightly woven fabric coated with polytetrafluoroethylene (PTFE), which serves as a vapor barrier to prevent condensation of moisture. Multiple layers of polyester foil coated with aluminum serve as radiation shields and give additional protection from the environment. An outer layer of polyvinyl chloride (PVC) in the form of pipe or a foil jacket provides secondary protection from the environment and protection against mechanical impacts. This system can be designed as a fully flexible blanket type configuration or a pre-formed molded type configuration for installation on a variety of cryogenic storage and transfer equipment.

This work was done by James E. Fesmire of **Kennedy Space Center** *and Jaesoek Ryu of Aspen Systems, Inc. For further information, please contact Kang P. Lee, President, Aspen Systems, Inc., 184 Cedar Hill Street, Marlborough, MA 01752.*

Inquiries concerning rights for the commercial use of this invention should be addressed to the Technology Programs and Commercialization Office, Kennedy Space Center, (407) 867-6373. Refer to KSC-11903.

Mechanics

Hardware, Techniques, and Processes

BLANK PAGE

Visualization of Flows in Beds Packed With Spheres

Flows were made visible by seeding and illumination with a sheet of laser light.

Lewis Research Center, Cleveland, Ohio

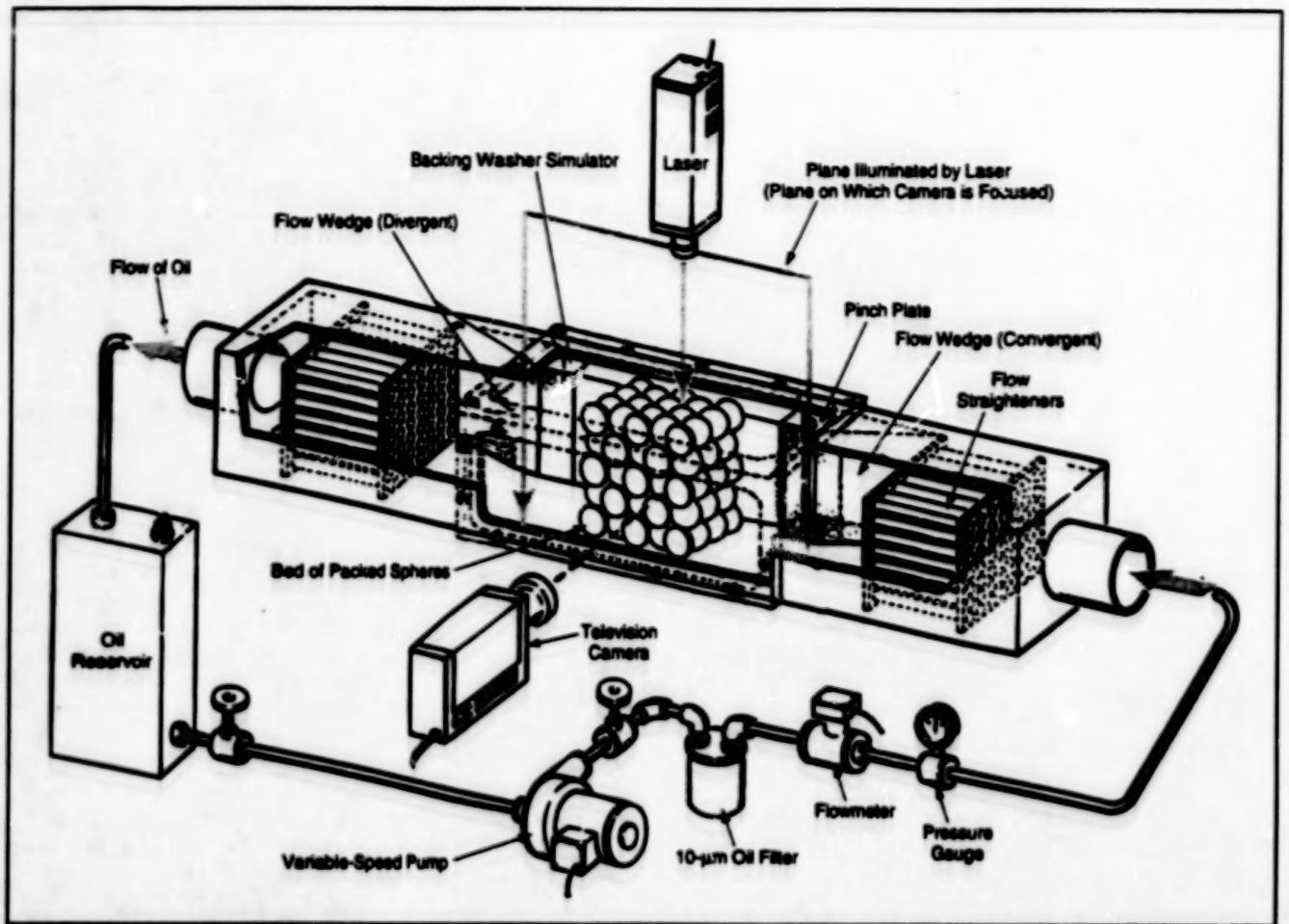

Oil Flowing in the Interstices of a bed of spheres was seeded with small particles and illuminated with a sheet of laser light to make the flow visible.

The figure shows an oil tunnel and associated equipment used in experiments, using the full-flow-field tracking (FFFT) technique, to characterize flows in beds packed with poly (methyl methacrylate) spheres. The indices of refraction of the oil and the spheres were matched to make the spheres invisible to the eye and cameras. The oil was seeded with magnesium oxide particles as flow tracers. The packed bed and the seeded oil in its interstices were illuminated with laser light in a plane aligned along the direction of bulk flow, thereby making visible some aspects of the flow dynamics. The image of the illuminated plane was recorded by a television camera aimed perpendicularly to the flow. The light sheet was traversed from one side of the tunnel to the other to acquire image data in different planes for use in synthesizing a three-dimensional image of the entire flow field.

The optical nature of the boundary interface between the working fluid and the spheres rendered the spheres black, permitting visualization of the exact locations of the circular oil/sphere interfaces in both the axial and transverse directions, with direct visualization of the complex interstitial spaces between the spheres within the bed. Strobing the laser provided a means to estimate the velocities of the flows within the bed of spheres and facilitated tracking the flow. Flows were observed near the planar tunnel walls and sets of spheres as well as near minor circles that appeared with great circles at various transverse positions and were not always uniformly ordered. The recorded images revealed very complex flow fields, and it was observed that flow channeling in the direction of bulk flow occurs between sets of adjacent spheres.

The flow was found to be fully three-dimensional and complex to describe. The most prominent finding involved conclusive experimental demonstration of flow threads as computed for hyper-cluster spheres in NASA Technical Memorandum 107361, "Numerical Flow Visualization in Basic- and Hyper-Cluster Spheres." More specifically, it was found that the bulk of the flow field has a natural tendency to establish the flow paths of least resistance (the above-mentioned threads) through the packed bed that are parallel and distinct and that for a regular array of spheres, the number of threads is related to the number of open areas in a cross section in a plane perpendicular to the direction of bulk flow.

Beds of spheres used in the experiments were constructed, variously, with regularly or randomly packed spheres of 12.7-mm or 19.05-mm diameter and were used to obtain various flow patterns. The effects of bed voids were also characterized and tended to disrupt flow threads and create vortices. Still photographs and video recordings that illustrate the flow phenomena are available.

This work was done by R. C. Hendricks of Lewis Research Center, S. Lattime of B & C Engineering, M. J. Braun of the University of Akron, and M. M. Athavale of

CFD Research Corp. Further information is contained in a TSP [see page 1].

Inquiries concerning rights for the commercial use of this invention should be addressed to NASA Lewis Research Center, Commercial Technology Office, Attn: Tech Brief Patent Status, Mail Stop 7–3, 21000 Brookpark Road, Cleveland, Ohio 44135. Refer to LEW-16562.

Smoother Wing Leading-Edge Joints Would Favor Laminar Flow

Appreciable reductions of drag should be achievable.

Ames Research Center, Moffett Field, California

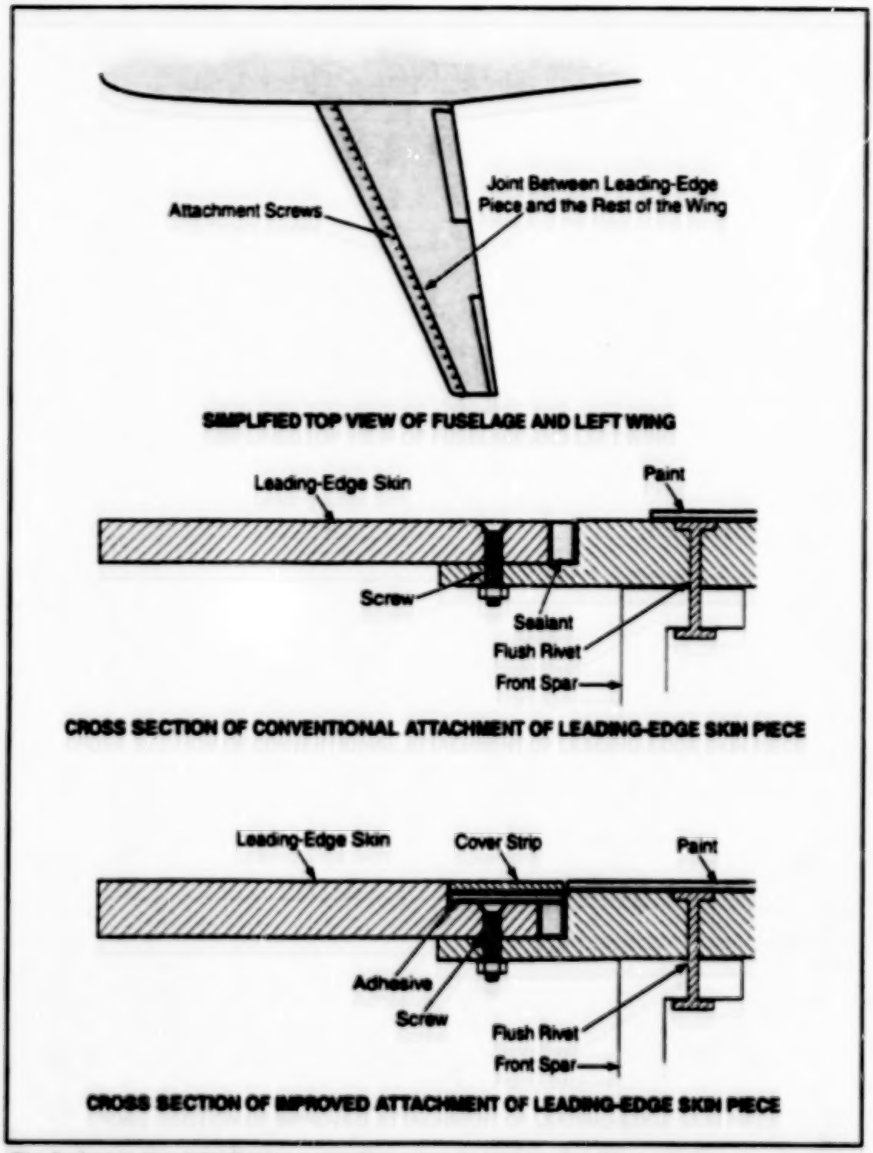

The Surface in the Joint Region is smoother when the leading-edge skin is attached according to the improved scheme. A smooth surface can support laminar flow, making it possible to obtain less drag than would be possible if surface discontinuities were allowed to trigger the transition to turbulent flow.

Some changes in the design and construction of the leading edges of metal airplane wings have shown promise as means to suppress laminar-to-turbulent flow transitions. The significance of this development is that it creates an opportunity to take advantage of laminar-flow boundary layers to reduce aerodynamic drag.

During the early 1950s, the aeronautical community reached a consensus to abandon laminar-flow drag-reduction techniques, in part because of a belief that practical metal airplane surfaces could not be made smooth enough to support laminar flow. The present development addresses an important aspect of the smoothness issue; namely, the interruption of the smooth wing surface at the joint between a leading edge and the rest of a wing. On a typical commercial jet airplane, each wing is constructed with a single-piece wraparound leading-edge skin piece attached to the rest of the wing by screws (see figure). The locus of attachment is a spanwise joint 4 to 6 in. (10 to 15 cm) downstream of the leading edge. The gaps and steps in the wing surface at the joint (including the exposed heads of the attaching screws) have been blamed for triggering laminar-to-turbulent flow transitions.

The present improved attachment scheme yields a joint smooth enough to support laminar flow. The improved scheme does not differ radically from the conventional scheme described above, does not require manufacturing accuracy significantly beyond that of conventional practice, and does not require expensive materials or expensive fabrication techniques. In the improved scheme as in the conventional scheme, the leading-edge skin piece is removable for infrequent inspection.

In the improved scheme, the leading-edge skin piece is made slightly thicker and a shallow recess is machined along the attachment region to allow for subsequent flush mounting of an aluminum or plastic cover strip. The cover strip is attached by use of a modern, easy-to-handle, commercially available high-strength adhesive; indeed, it is only the advent of such adhesives that has made it practical to implement the present scheme. The edges of the strip can be trimmed carefully so that the remaining gaps are smaller than a critical dimension for triggering the laminar-to-turbulent transition.

The efficacy of the improved scheme, has been verified in flight tests: A test fixture designed to reproduce a wing surface according to the improved scheme, with various simulated degrees of manufacturing precision, was mounted on an airplane and flown at representative mach and Reynolds numbers. Laminar flow was observed, and a readily available foam-backed adhesive held the cover strip in place with no sign of failure.

This work was done by Robert A. Kennelly, Jr., Dennis J. Koga, and Fanny A. Zuniga of **Ames Research Center;** *Aaron Drake of San Jose University State; Michael L. Hinson of Learjet, Inc.; and Russell V. Westphal of Washington State University. No further documentation is available.*

Inquiries concerning rights for the commercial use of this invention should be addressed to the Patent Counsel, Ames Research Center [see page 1]. Refer to ARC-14088.

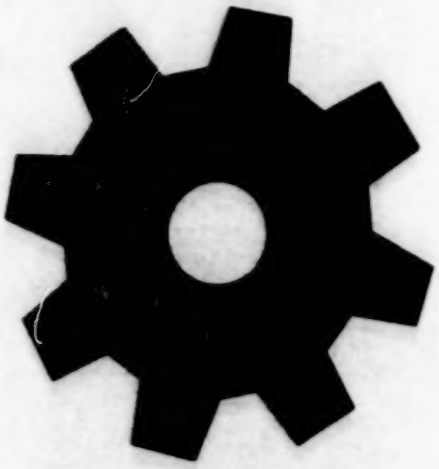

Machinery

Hardware, Techniques, and Processes

BLANK PAGE

Improved Inlets for T-38 Airplane

The change in inlet design reduces takeoff distances and increases safety margins.

Lyndon B. Johnson Space Center, Houston, Texas

A change in the design of the engine inlets of the T-38 airplane significantly reduces takeoff distances while increasing safety margins. Although the newer inlet design (see Figure 1) is based on well-known engineering principles, it is unique and will prove invaluable to the NASA fleet and to other T-38 fleets; e.g., the fleets flown by the United States Air Force (USAF) and by foreign governments. The change in design was needed because in an inlet of the older design, separation of flow in the lower third of the inlet degraded efficiency, even under normal takeoff conditions. Johnson Space Center (JSC) engineers compensated for this deficiency in formulating the newer design by adopting an inlet shaped according to aerodynamical considerations; the shape was chosen to minimize separation of flow to produce greater engine thrust as the T-38 accelerates to takeoff speed.

Figure 2 depicts an aspect of the older and newer inlet shapes. The older design, developed in the late 1950s, was optimized for supersonic flight. However, both the NASA and USAF missions for the T-38 now emphasize subsonic flight, in which the older inlet design causes internal separation from incoming air. This separation starves the engines of air, thereby reducing engine efficiency. The consequences of reduced engine efficiency include increases in takeoff distances, decreases in safety margins, and engine failures that result in higher-risk, single-engine takeoffs.

Figure 1. The Improved T-38 Engine Inlet design affords enhanced performance and safety. NASA's T-38 fleet will be modified to incorporate this design. The USAF T-38 fleet and the fleets of foreign countries can be similarly modified.

At such hot, high-altitude airports as the one at El Paso, Texas, the risk is even greater. Because of climatic conditions and the relative thinness of the atmosphere there, especially in summer, T-38s cannot take off at full weight. Fuel must be burned off, or flight crews must wait until surface temperatures fall sufficiently to permit takeoff. Such extremes produce a Category III condition; that is, a condition in which critical field length exceeds runway length, reducing the accepted measure of takeoff performance. JSC engineers addressed this condition in changing the inlet design.

The JSC design was not the only alternative considered. The older inlet might have been modified with auxiliary, moveable doors that could open for takeoff to allow more air to enter the engines. However, this modification would have (1) increased aircraft weight by 120 lb (54 kg), posing a sizeable risk at El Paso and

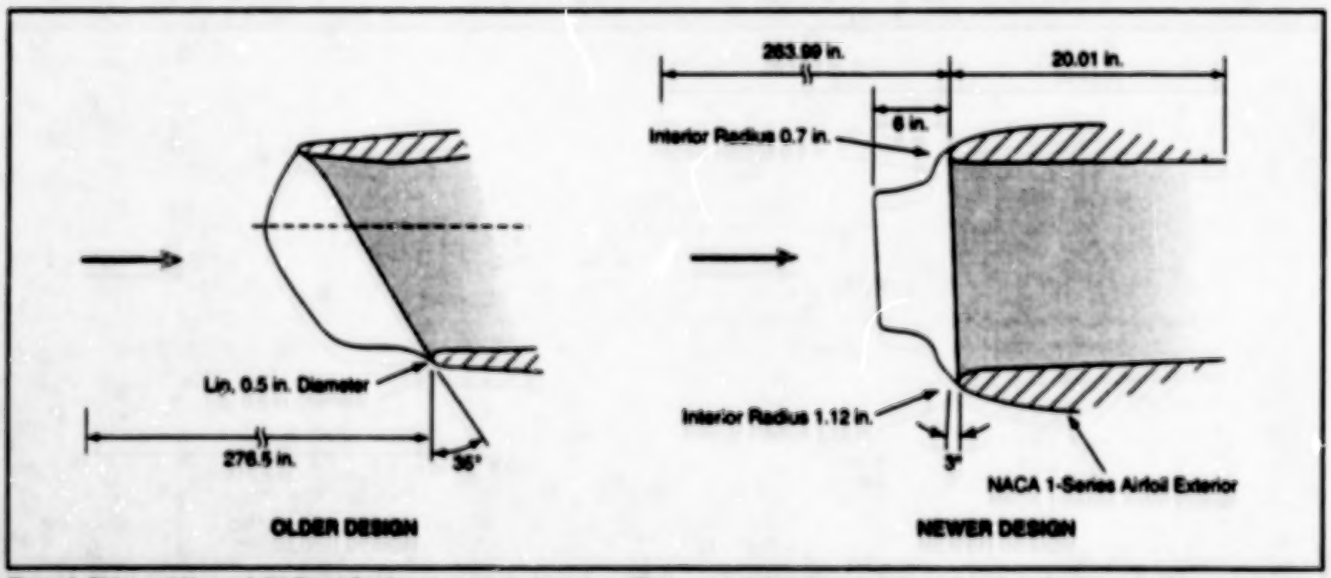

Figure 2. Older and Newer Inlet Cross Sections in a longitudinal plane differ in ways that translate to better subsonic performance for the newer design.

other locations where weight is already of concern; and (2) increased the T-38 life-cycle cost, owing to required maintenance on the modified inlet.

By enlarging the area of the inlet and significantly thickening the inlet, JSC engineers developed an inlet design that promotes laminar flow of incoming air, increasing aircraft efficiency and thrust. The exterior profile was customized for maximum aerodynamic performance and to maintain continuity with existing aircraft structures. Because there are no moving parts, the increase in weight associated with the modification is negligible [approximately 10 lb (≈4.5 kg)]. Clearly, the JSC inlet for T-38 aircraft offers a superior alternative to both the older design and to the auxiliary-door proposal.

NASA's T-38 fleet will be modified to incorporate the newer design. The USAF T-38 fleet and the fleets of foreign countries can be similarly modified.

This work was done by Robert Ess and David Eichblatt of **Johnson Space Center**. *No further documentation is available.*
MSC-22785

The X-36 Program: A Test Pilot's Perspective on UAV Development Testing

A test pilot shares his experience with this unique aircraft.

Dryden Flight Research Center, Edwards, California

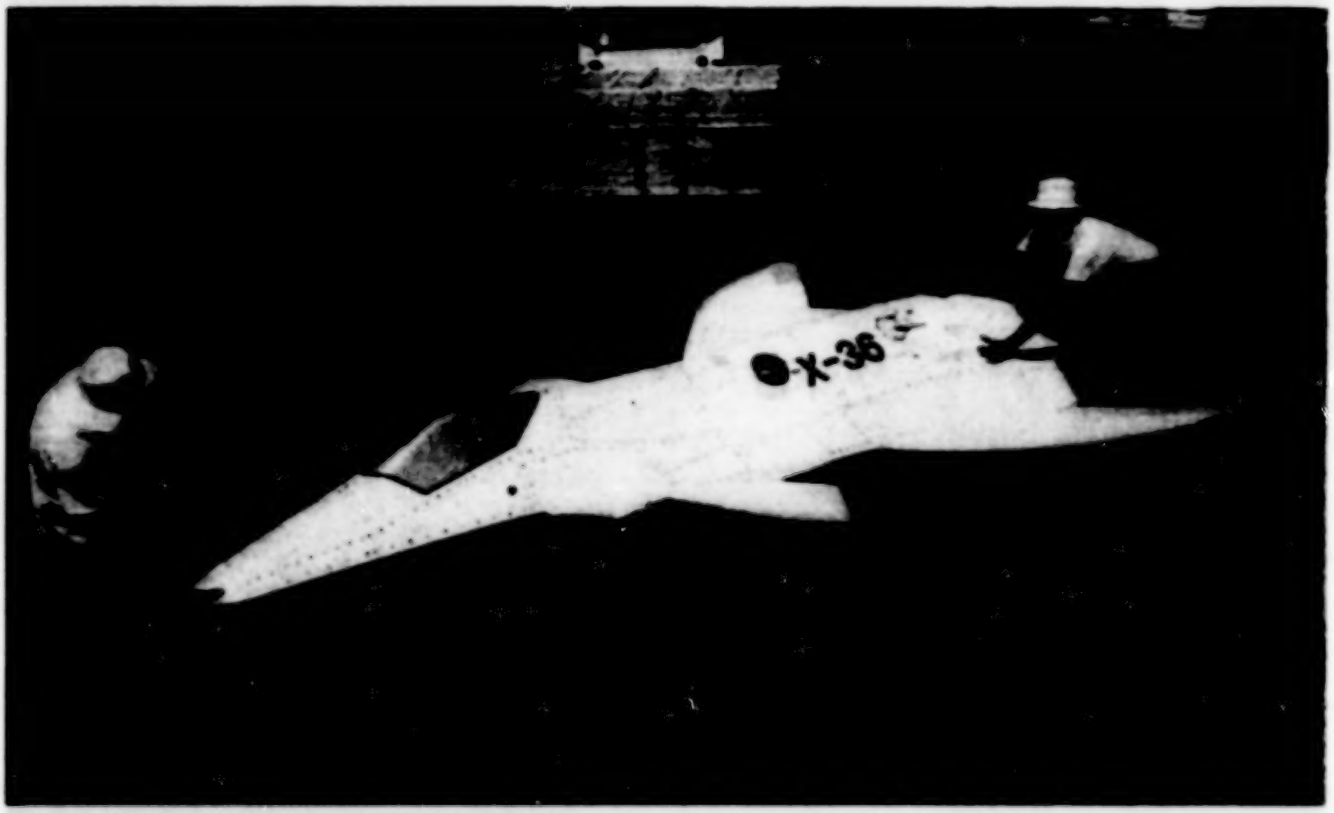

The X-36 UAV is being rolled out of a hangar for a flight test.

The Dryden Flight Research Center (DFRC) has been a partner in many uninhabited-aerial-vehicle (UAV) test programs. Our participation has largely been in the areas of technical oversight and range safety, but the X-36 program provided an opportunity to get some "stick and throttle" experience in this very unique type of flying. It was also an excellent opportunity to evaluate first hand the elements which make a successful UAV test program. I participated in the program as part of an independent review team, a chase pilot, and as a project pilot. In November 1997, I piloted two parameter-identification and flight-envelope-expansion sorties — they proved to be some of the most intense flight testing of my career.

The X-36 is a 28-percent scale, remotely piloted research aircraft (see figure) designed to develop tailless, high angle of attack, fighter agility with a stealth design. It uses a control system consisting of canards, split ailerons, leading and trailing edge flaps, and thrust vectoring. The aircraft length is nearly 18 ft (5.5 m), the wingspan is about 11 ft (3.4 m) and the takeoff weight is approximately 1,250 lb (567 kg). It is powered by a Williams International F-112 turbojet engine with approximately 700 lb (318 kgf) of thrust. The flight operations were conducted from a control trailer, which contained both control-room stations and the pilot cockpit.

The cockpit controls and displays were designed to emulate a standard fighter type aircraft cockpit. The controls included a displacement stick, rudder pedals, a throttle quadrant, and several instrument-panel pushbutton switches. All normal flight functions could be controlled from the buttons on the stick and throttle (HOTAS). Two 20-in. (0.51 m) color displays were used to display information. One had the "out-the-nose" picture from the on-board video camera, with heads-up display (HUD) symbology overlaid to obtain a true 1:1 correlation

with the video imagery. The second screen had a map indicating the location of the aircraft in the test area and numerous system-status and warning indicators. Finally, a microphone located inside the aircraft provided some valuable audio information on aircraft systems and engine performance.

Piloting the X-36 is an intensely visual task. Gone are the large field of regard, the subtle "seat-of-the-pants" inputs and numerous audio clues which normally allow the test pilot to have better situational awareness than anyone else on the test team. Instead, the pilot must rely on a rapid and focused cross check of his/her displays and precise communications with the test conductor. To aid concentration, the pilot was isolated from the rest of the control room area by a curtain and his communications were restricted to the flight director and radio traffic using a separate "flight loop" intercom set up. Behind the pilot was a position which allowed another pilot/engineer to view the displays. This position proved useful for both pilot training and for providing "copilot type" assistance to the flying pilot.

The display symbology needed to meet two conflicting requirements. First, it had to provide enough information to the pilot, in an intuitive format, to compensate for the lack of audio and physical cues discussed previously. Second, the symbology needed to be uncluttered enough to allow the pilot to find and assess quickly key flight parameters. During rapid maneuvering, it was often desired to track airspeed, angle of attack, bank angle, and normal acceleration precisely, while looking for any indication of sideslip or angle-of-attack excursions, engine-compressor stalls, and the like. The X-36 symbology was developed primarily by the chief contractor pilot and reflected his experience with F-15 and F-18 aircraft. I found the symbology very complete, but often too cluttered and a large portion of my training was devoted to finding the correct cross check for each maneuver block. The tailoring of symbology is an issue in all types of aircraft, but for an RPA, the correct symbology set is often critical to flight safety and mission success.

The key to my success with these sorties was the 10 hours of high-fidelity simulation training I obtained prior to an actual takeoff. I "piloted" the aircraft from the actual RPA cockpit with the most current aircraft model and a simulated out-the-nose visual presentation. Both normal and emergency operations were practiced until I was proficient. The simulator training culminated in a full test mission practice prior to the actual flight. Additional training included an actual engine start and a high-speed taxi test to 70 kn on the lakebed runway.

The test flights closely followed the simulator training. The takeoff was accomplished from lakebed runway 15 and the aircraft quickly climbed into the test airspace. Basic aircraft control was easily accomplished using the HUD symbology and the video image. The test maneuvers included a series of control-stick and rudder-pedal rolling maneuvers at various airspeeds and angles of attack. Several level accelerations were accomplished to expand the speed envelope of the aircraft. The aircraft exhibited excellent flying qualities throughout the flight. All the rolls were rapid and the bank-angle/angle-of-attack targets were precisely tracked. The aircraft was able to change speed rapidly, and the lack of any audio or physical speed cues, required the pilot to spend extra attention to this display.

Perhaps the most challenging part of the flight was the landing pattern. Airspace restrictions forced us to use a continuous turn to final which meant that the runway was not in sight until very late in the approach. The turn was made using the moving map display to insure the correct offset. This maneuver required the use of almost all the information presented to the pilot. The landing was accomplished by simply establishing an on-speed descent at about 1 degree. The aircraft would smoothly touchdown, and ground control and braking were very easy.

My experience with this program confirmed my belief that successful development and flight testing of a UAV requires the same discipline and expertise as any other aircraft. Years of flight test experience have defined a set of "flight test best practices". Simply stated, these embody the attitude and the processes which have proven to be critical to mission success. A few of the key points are:

1. Robust Designs and Quality Construction – A major "benefit" of going with a UAV is the ability to simplify the systems of the vehicle. However, simple, nonredundant systems demand careful design to reduce the effect of failures. A "graceful degradation" of system performance is desired. Critical "single string" systems (such as flight controls) are only successful when supported by high-quality parts and construction. "Off-the-shelf" technologies which are integrated into a new vehicle do not insure low-risk flight operations.
2. Hazard Analysis – The failure of the UAV prior to meeting its mission objectives is unacceptable. The hazard analysis must properly identify the probability and the severity of the hazards the vehicle may encounter. Once identified, steps must be taken to mitigate each of the hazards to the lowest level possible. Only then can the program present to management the true level of risk that must be accepted during flight test.

Also, the program must avoid the "expendability mind-set," which accepts that UAVs fail at a higher rate than other aircraft. This attitude may result in accepting a substandard system or procedure. Today's UAVs are not often cheap, throw-away aircraft. They are sophisticated, expensive, and often one-of-a-kind aircraft, the damage or loss of which has a major impact on the mission success of the program.

3. Configuration Control – The hardware and software of the system will always change during the course of development. A well designed and built vehicle cannot maintain its high standard without a process for identifying and controlling changes to the baseline.
4. Test Planning and Test Mission Conduct – Programs need to recognize that flight test personnel can make valuable inputs to the design of the entire system. Often, the best engineering choice is the one which satisfies the operational requirements for the vehicle and the flight tester usually has the most experience in this area. Also, it is important to recognize that it is normally unacceptable to take "short cuts" in the flight test process. Flight safety and mission success are seriously impacted by the omission of any of the "best practices" discussed.

Overall, the X-36 program was both challenging and educational. In my opinion, it is an excellent example of how to conduct UAV developmental flight test.

This work was done by Dana D. Purifoy of **Dryden Flight Research Center**. *Further information is contained in a TSP [see page 1].*
DRC-97-55

Robot Arm Actuated by Electroactive Polymers

The actuators function similarly to components of human arms and hands.

NASA's Jet Propulsion Laboratory, Pasadena, California

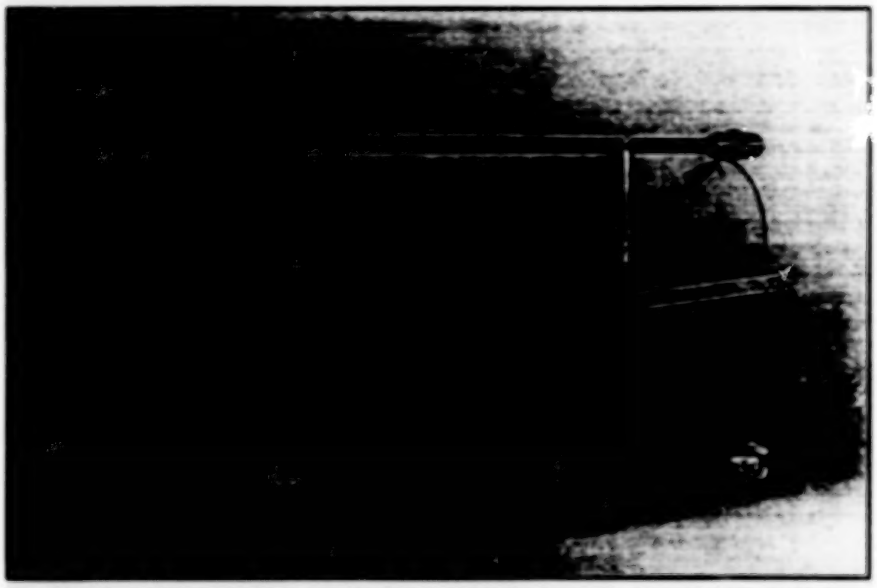

This Miniature Crane has been used to demonstrate the feasibility of small, lightweight, low-power-consumption robot arms containing electroactive-polymer actuators. In an experiment, the crane lifted a rock by 3/4 in. (19 mm). It should be possible to increase the lifting distance by optimizing the design of the ropelike LEAs.

The figure shows a robot arm that is essentially a miniature crane actuated by electroactive polymers. This mechanism has been constructed as part of a continuing effort to develop lightweight, compact, low-power-consumption telerobots.

Electroactive polymers have been chosen as the actuator materials for this development because they offer advantages over such competing actuator materials as electroactive ceramics (both piezoelectric and electrostrictive). For example, whereas the maximum actuation strains of electroactive ceramics range between 0.1 and 0.3 percent, those of electroactive polymers exceed 10 percent; and whereas the densities of electroactive ceramics range from is 4 to 6 g/cm^3, those of electroactive polymers range from 1 to 2.5 g/cm^3. Electroactive polymers can be formed into almost any shape, are flexible and tough, and damp vibrations. Like other polymers, electroactive polymers can be mass-produced at relatively low cost. Unlike piezoceramics, electroactive polymers need not be poled during manufacturing; this helps keep production costs low.

The lever arm of the miniature crane is a hollow graphite/epoxy rod 15 in. (38.1 cm) long, with an inner diameter of 1/4 in. (6.4 mm) and an outer diameter of 1/3 in. (8.5 mm). The pivot point divides the rod into two parts with length ratio of 5:1. The electroactive-polymer actuators are of two types:

- There are two linear electrostatic actuators (LEAs). These are ropelike objects made from an electrostatically activated polymer (a silicone) with carbon surface coats as electrodes. LEAs function analogously to muscles in that they act by shortening or lengthening. One of the LEAs lies along the top and over the outer end of the longer part of the lever arm, where it hangs down and holds a gripper. The other LEA is fastened between a fixed point and the outer end of the shorter part of the lever arm. The two LEAs are electrically activated in synchronism so that their actuation effects add to maximize the stroke in lifting or lowering an object held by the gripper.
- The gripper contains four fingers that are not jointed but nevertheless bend and thus function similarly to human fingers. The fingers are perfluorinated-ion-exchange-membrane/platinum composites. When a voltage is applied across the thickness of such a finger, electrostriction in the ion-exchange polymer in the membrane causes the finger to bend; the direction of bending depends on the polarity of the voltage. Hooks on the ends of the fingers help to secure the grip on the object, which can be picked up and carried once the fingers close around it. [The gripper was described previously in more detail in "Robot Hands With Electroactive-Polymer Fingers" (NPO-20103) NASA Tech Briefs, Vol. 22, No. 10 (October 1998), page 78.]

This work was done by Yoseph Bar-Cohen and Tianji Xue of Caltech, and Brian Lucky, Cinkiat Abidin, Marlene Turner, and Harry Mashhoudy of UCLA for **NASA's Jet Propulsion Laboratory**. *Further information is contained in a TSP [see page 1].*

NPO-20393

Mathematics and Information Sciences

Hardware, Techniques, and Processes

BLANK PAGE

Computer Network for Distribution of Radiographic Images

The network would also be used for training in radiography.

John F. Kennedy Space Center, Florida

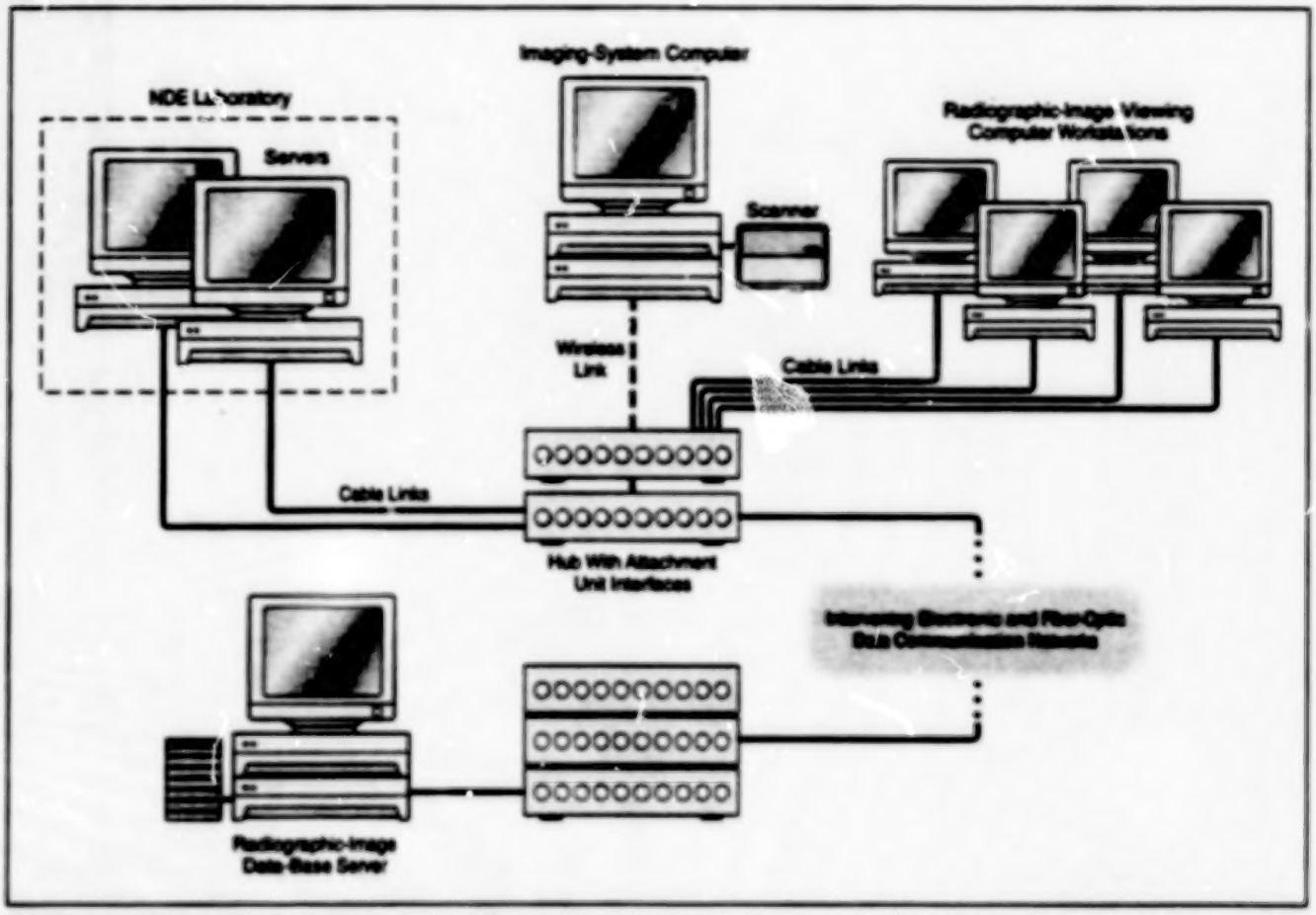

The Radiographic Imaging Performance Support System is a developmental computer network for centralized storage, retrieval, and analysis of radiographic images, without need to distribute original radiographic films.

The Radiographic Imaging Performance Support System (RIPSS) is a developmental computer network intended to serve as (1) a central electronic archive for the storage, retrieval, and analysis of radiographic images generated in nondestructive-evaluation (NDE) laboratories at Kennedy Space Center and (2) a system for training users in radiographic techniques and in the analysis and interpretation of radiographic images. The archival, analytical, and training subsystems are being developed concurrently and integrated to the extent possible to take advantage of synergies among them and thereby maximize the potential to enhance the performances of both NDE learners and practicing NDE professionals.

The RIPSS would supplant the present system, in which there is no central archive, and in which both analysis and training are impeded by the need to distribute original radiographic films for comparison. The RIPSS (see figure) would include a scanner and a data-base server computer, which would store the digitized information from the original radiographic films, making it unnecessary to handle the films after scanning them. Storage of the image information in electronic form would reduce the cost of distribution, provide some redundancy for protection against loss, provide systematic means for preventing access by unauthorized users, and enable the use of automated computational techniques for retrieval and analysis.

The subsystems for storage, retrieval, and analysis of images would incorporate object-oriented data structures and Internet-based multimedia formats for efficiency in development and deployment. Large multimedia files (for example, files containing images with text and audio annotations) could be accommodated. Advanced file-management features would be provided. One particularly notable feature of this type is the query by image contents (QBIC), which can be implemented with commercially available software. For example, if a specific section of pipe were tested on several occasions and its radiographic image scanned into the system on each occasion, then subsequent retrieval of one of the images would facilitate access to all like images. The software would find all images of segments of pipe having the same bend. The search could be narrowed by use of various parameter filters. This feature could be an excellent tool for the comparative analyses that are often performed in analyzing radiographic images.

The training subsystem of the RIPSS is based partly on the Kennedy Space Center developed "Web Interactive Training" where the capabilities afforded by the Internet and by state-of-the-art multimedia data-presentation techniques are exploited to deliver training from a server computer to client desktop computers on demand. Training can be interactive, and interactivity can be exploited to provide for testing and recording of a trainee's progress. The fully developed RIPSS would enable a trainee or other user to visually inspect a radiograph and to click

on a section containing a discontinuity suspected to represent a defect. Underlying image-map coordinates would direct the user to a page that would describe the discontinuity and present case-study information about the radiograph. The user interface for both training and routine use in inspection of parts would be the same.

This work was done by Alexander H. Ladd formerly of I-NET, Inc., and David Metcalf of Merrimac Interactive Media Corporation for **Kennedy Space Center.** *Further information is contained in a TSP [see page 1].*

Inquiries concerning rights for the commercial use of this invention should be addressed to the Technology Programs and Commercialization Office, Kennedy Space Center, (407) 867-6373. Refer to KSC-12000.

Program Estimates Run Time on a Parallel Computer

The main advantage of this program is relative simplicity and speed.

NASA's Jet Propulsion Laboratory, Pasadena, California

The Pathcalc computer program estimates the time needed to execute a given application program on a parallel computer of given computation and network capabilities. Pathcalc can be used to analyze the effects of changes in such parameters as central-processing-unit (CPU) speed, network bandwidth, and network latency. Pathcalc is written in Java and should be executable on most computers.

Pathcalc could be used to determine how long it would take to execute the same application program on a different parallel computer or whether a specified faster network or a faster CPU could execute the program in an acceptably short time. It could also be used to determine what part of a parallel system is slowing down execution of a given application program the most: For example, by artificially setting the CPU speed very high, one could determine how much time is used in communication; or by artificially setting the communication speed very high, one could determine how much time is consumed in CPU operations.

It is not necessary to understand the application program or to mathematically model the network in order to use Pathcalc. All one needs is the trace files (one such file for each CPU of the computer) from a previous run of the application program. Pathcalc then generates its estimate on the basis of the trace files and the network parameters provided by the user.

The estimate is valid only (1) for a computer with the same number of nodes used to generate the trace files; (2) provided that message passing is restricted to such simple routines as send, receive, and barrier calls; and (3) provided that the execution of the application program can be relied upon to always follow the same path through the code, regardless of changes in network response times. In situations in which these restrictions are acceptable, Pathcalc offers advantages of simplicity and speed over a number of other programs that estimate execution times of application programs; this is because unlike those estimators, Pathcalc uses only the trace information instead of executing the application programs themselves.

This work was done by Paul Springer of Caltech for **NASA's Jet Propulsion Laboratory.** *Further information is contained in a TSP [see page 1].*
NPO-20237

Automated Scheduling and Reporting of Fire Inspections

A computer-based automated system for scheduling, reporting, and tracking fire inspections at Kennedy Space Center has supplanted a manual system based on paper fire-inspection reports transmitted by mail. The automated system not only minimizes the consumption of paper and other resources but also significantly reduces the time spent in responding to potentially hazardous conditions. The software in the automated system generates a multiscreen interactive display containing standard fire-inspection report forms. Inspectors check off predefined items, fill in blanks, and/or enter text, as needed, to complete the forms. The information thus entered is stored in a data base. Automated mail-merge documents are created and transmitted to responsible site managers by electronic mail. Inspections are tracked by a report section that identifies overdue corrective actions and prompts follow-up by a fire inspector or supervisor. Although this software was originally written for fire inspections, it is easily adapted for nearly any inspection process, i.e., safety, environmental, etc., since all "predefined" items can be defined at setup.

This work was done by Hans J. Siepmann formerly of EG&G Florida, Inc., for **Kennedy Space Center.**

Inquiries concerning rights for the commercial use of this invention should be addressed to the Technology Programs and Commercialization Office, Kennedy Space Center, (407) 867-6373. Refer to KSC-12050.

Planning and Resource Reasoning Software

"Planning and Resource Reasoning" ("PARR") is the name now applied to a scheduling methodology and to computer programs developed to implement the methodology during the years 1985 through 1987. In PARR, one uses heuristics and reactive techniques to build schedules. PARR software is generic enough to be useable in almost any scheduling application in which electronic representations of the resources to be scheduled are available, and in which constraints and conflict-resolution strategies can be represented in terms of heuristics. PARR software takes much less time to produce schedules than do programs that produce optimized schedules. Although PARR-generated schedules are suboptimum, they are acceptable and they satisfy the specified constraints. PARR software can be run in a batch mode for initial generation of schedules, or in an interactive mode for refinement of previously generated schedules.

This work was done by David Richard McLean of Allied Signal for **Goddard Space Flight Center.** *Further information is contained in a TSP [see page 1].*
GSC-14097

END

12-13-99